



HAL
open science

Water in Omphacite and Garnet From Pristine Xenolithic Eclogite: T - X - f O₂ Controls, Retentivity, and Implications for Electrical Conductivity and Deep H₂O Recycling

Sonja Aulbach, Roland Stalder, Malcolm Massuyeau, Richard Stern, Dmitri Ionov, Andrey Korsakov

► To cite this version:

Sonja Aulbach, Roland Stalder, Malcolm Massuyeau, Richard Stern, Dmitri Ionov, et al.. Water in Omphacite and Garnet From Pristine Xenolithic Eclogite: T - X - f O₂ Controls, Retentivity, and Implications for Electrical Conductivity and Deep H₂O Recycling. *Geochemistry, Geophysics, Geosystems*, 2023, 24 (12), 10.1029/2023GC011170 . hal-04732175

HAL Id: hal-04732175

<https://hal.science/hal-04732175v1>

Submitted on 12 Oct 2024

HAL is a multi-disciplinary open access archive for the deposit and dissemination of scientific research documents, whether they are published or not. The documents may come from teaching and research institutions in France or abroad, or from public or private research centers.

L'archive ouverte pluridisciplinaire **HAL**, est destinée au dépôt et à la diffusion de documents scientifiques de niveau recherche, publiés ou non, émanant des établissements d'enseignement et de recherche français ou étrangers, des laboratoires publics ou privés.



Distributed under a Creative Commons Attribution - NonCommercial - NoDerivatives 4.0 International License

Geochemistry, Geophysics, Geosystems®



RESEARCH ARTICLE

10.1029/2023GC011170

Key Points:

- Electrical conductivity in deep (>100 km) pristine eclogite xenoliths from Siberian and Slave cratons increases with depth
- H₂O content increases with Al₂O₃, which is highest in gabbroic eclogites with deep oceanic crustal protoliths
- The H₂O content of subducted bulk oceanic crust sampled by eclogite 3 Ga ago may be similar to today

Supporting Information:

Supporting Information may be found in the online version of this article.

Correspondence to:

S. Aulbach,
s.aulbach@em.uni-frankfurt.de

Citation:

Aulbach, S., Stalder, R., Massuyeau, M., Stern, R. A., Ionov, D. A., & Korsakov, A. V. (2023). Water in omphacite and garnet from pristine xenolithic eclogite: *T-X-fO₂* controls, retentivity, and implications for electrical conductivity and deep H₂O recycling. *Geochemistry, Geophysics, Geosystems*, 24, e2023GC011170. <https://doi.org/10.1029/2023GC011170>





Received 10 AUG 2023
Accepted 8 NOV 2023

Author Contributions:

Conceptualization: Sonja Aulbach
Formal analysis: Sonja Aulbach, Malcolm Massuyeau, Richard A. Stern
Funding acquisition: Sonja Aulbach
Investigation: Sonja Aulbach, Richard A. Stern
Methodology: Roland Stalder, Malcolm Massuyeau, Richard A. Stern
Project administration: Sonja Aulbach
Resources: Roland Stalder

© 2023 The Authors. *Geochemistry, Geophysics, Geosystems* published by Wiley Periodicals LLC on behalf of American Geophysical Union. This is an open access article under the terms of the [Creative Commons Attribution-NonCommercial-NoDerivs License](https://creativecommons.org/licenses/by/4.0/), which permits use and distribution in any medium, provided the original work is properly cited, the use is non-commercial and no modifications or adaptations are made.

Water in Omphacite and Garnet From Pristine Xenolithic Eclogite: *T-X-fO₂* Controls, Retentivity, and Implications for Electrical Conductivity and Deep H₂O Recycling

Sonja Aulbach¹ , Roland Stalder², Malcolm Massuyeau³, Richard A. Stern⁴ , Dmitri A. Ionov⁵ , and Andrey V. Korsakov⁶ 

¹Institut für Geowissenschaften, Goethe-Universität Frankfurt, Frankfurt, Germany, ²Universität Innsbruck, Institut für Mineralogie und Petrographie, Innsbruck, Austria, ³Institute for Mineralogy, University of Münster, Münster, Germany, ⁴Canadian Centre for Isotopic Microanalysis, Department of Earth and Atmospheric Sciences, University of Alberta, Edmonton, AB, Canada, ⁵Geosciences Montpellier, University of Montpellier, Montpellier, France, ⁶Sobolev Institute of Geology and Mineralogy, Siberian Branch, Russian Academy of Science, Novosibirsk, Russian Federation

Abstract Kimberlite-borne eclogite xenoliths having Precambrian oceanic crustal protoliths and entrained from ≥100 km depth can retain pristine geochemical features despite extended residence in the cratonic lithospheric mantle, making them valuable archives of deep chemical cycling including that of water. We determined, by Fourier Transform Infrared Spectroscopy, structural OH contents in clinopyroxene and garnet from 15 unmetasomatized eclogite xenoliths. Calculated total c(H₂O) is 100–510 wt.ppm for clinopyroxene and below detection (~2 wt.ppm) to 200 wt.ppm for garnet, while garnet δ¹⁸O, determined by Secondary Ion Mass Spectrometry, ranges from +5.0‰ to +7.3‰, (similar to high- and low-temperature seawater-altered oceanic crust). Estimated electrical conductivity in pristine eclogites increases with temperature (i.e., depth for conductive geotherms), while clinopyroxene-garnet H₂O partition coefficients decrease with increasing temperature and garnet grossular component (i.e., Ca#), similar to other incompatible components. Various considerations suggest the retention of primary H₂O in the samples, likely occurring in km-sized pods of coarse-grained eclogite. High Al₂O₃ in clinopyroxene as omphacite component, stabilized during high-pressure metamorphism, facilitates H₂O uptake. Therefore, the high bulk c(H₂O) estimated for samples with plagioclase-rich, deep crustal protoliths (median 290 wt.ppm) may indicate an interaction with fluids expelled at depth from serpentinites. The c(H₂O) of ancient and modern subducted bulk oceanic crust (~220–240 wt.ppm) are similar, suggesting constant mantle ingassing since at least 3 Ga ago. This places constraints on factors, such as mantle temperatures, that determine the efficiency of deep water cycling.

Plain Language Summary Water in Earth's interior exists mostly as OH⁻ anion in trace abundances in nominally anhydrous minerals. Despite these low concentrations, deep water exerts a strong influence on fundamental Earth processes, such as partial melting of the mantle and the operation of plate tectonics. However, the extent to which the loss of water via volcanism has been compensated over time by retention in downgoing oceanic plates, after their dehydration and metamorphism to eclogite, remains poorly known. Deeply buried Archean and Paleoproterozoic oceanic crust is sampled as remarkably pristine eclogite fragments quickly exhumed by volcanism from depths >100 km. High Al₂O₃ contents, characteristic of deep crustal plagioclase-rich cumulates, facilitate H₂O-uptake in clinopyroxene, the main carrier of H₂O in eclogite. Because clinopyroxene is rich in Al only at high pressure, where the crust is already dehydrated, but the underlying seawater-altered mantle begins to liberate fluids, we suggest that interaction with this fluid explains the Al-H₂O association. Moreover, the eclogite-based H₂O estimate for ancient crust is similar to estimates for the modern crust, suggesting that deep water cycling in the crustal part of subducting slabs changed little in the last 3 billion years, with consequences for the factors determining the efficiency of ingassing.

1. Introduction

The continental mantle lithosphere is predominantly composed of peridotite, but contains a subordinate amount of eclogite and pyroxenite distributed as pods, lenses, or layers, the majority of which originated as subducted oceanic crust (Aulbach & Jacob, 2016; Jacob, 2004). Observational data, thermodynamic models and experimental constraints indicate an origin of xenolithic eclogite as spreading ridge-derived and variably differentiated oceanic crust that was subsequently exposed to varying degrees of seawater alteration followed by dehydration,

Validation: Sonja Aulbach, Roland Stalder, Malcolm Massuyeau, Richard A. Stern

Visualization: Sonja Aulbach

Writing – original draft: Sonja Aulbach

Writing – review & editing: Roland Stalder, Malcolm Massuyeau, Richard A. Stern, Dmitri A. Ionov, Andrey V. Korsakov

partial melting and interaction with slab-derived fluids during recycling in Paleoproterozoic (Slave) and Archean (Siberian, Kaapvaal) subduction zones (Aulbach & Smart, 2023). Even though they represent a subordinate lithology, eclogites in the mantle, with their distinct chemical and modal compositions, hence geophysical properties, cannot be neglected in models of continental lithosphere mantle state and structure (Garber et al., 2018). The electrical conductivity of eclogites is also critical for understanding and interpreting magnetotelluric signatures that integrate over the bulk lithosphere (e.g., Jones et al., 2009; Selway, 2014). Structurally bound hydrogen, even at trace levels in nominally anhydrous minerals (NAMs) is conventionally referred to as “water” and reported as wt.ppm H₂O (e.g., Demouchy & Bolfan-Casanova, 2016; Peslier et al., 2017). Water plays a particular role in the longevity of continental lithosphere as its presence affects phase relations, rheology and deformability (e.g., Green et al., 2010; Kohlstedt, 2006), and it has been strongly implicated in craton destruction via the removal of deep lithospheric roots (e.g., Peslier et al., 2010; Xia et al., 2019). As omphacite is a major carrier of H₂O and eclogite is composed of subequal proportions of clinopyroxene and garnet, eclogites ought to be a significant H₂O reservoir in the mantle (e.g., Katayama et al., 2006; Skogby et al., 1990; Smyth et al., 1991).

Moreover, despite its residence in the cratonic lithosphere for billions of years, eclogite sampled as xenoliths in kimberlites and lamproites can retain surprisingly pristine compositions. For example, some samples with marked plagioclase signatures (strong positive Eu anomalies and high Al₂O₃, low FeO and ΣREE abundances) have exceptionally unradiogenic Sr (<0.7010) and low bulk Fe³⁺/ΣFe (<0.05), which reflects their origin as cumulates depleted in Rb and ferric Fe due to their lower compatibility relative to Sr and ferrous Fe, suggesting relatively undisturbed evolution until entrainment (Aulbach & Arndt, 2019; Aulbach et al., 2022). While orogenic eclogites may host much water in NAMs (e.g., Katayama et al., 2006), it is becoming increasingly clear that exhumed metamorphic rocks are not representative of the total subducted lithosphere (e.g., Penniston-Dorland et al., 2015; Y. Wang et al., 2023). This potentially leaves eclogite xenoliths as our best source for robust models of hydrogen ingassing beyond sub-arc depths for conditions relevant to oceanic crust in ancient subduction zones. Such models are based on thermochemical considerations, high-pressure experiments (mostly on phase relations of hydrous minerals), or geophysical observations (e.g., Jarrard, 2003; Magni et al., 2014; Paulatto et al., 2017; Rüpke et al., 2004; Schmidt & Poli, 2014; van Keken et al., 2011). However, despite sporadic studies, H₂O content in xenolithic eclogite remains poorly known.

To address the paucity of constraints on H₂O content in the mantle eclogite reservoir, we report H₂O contents in omphacite ± garnet in pristine (non-metasomatized) eclogite xenoliths from the Siberian and Slave craton (*n* = 15). We seek to test to what extent H₂O contents in eclogite xenoliths exhumed from their lithospheric mantle sources often billions of years after their emplacement in Archean (Siberia) and Paleoproterozoic (Slave) subduction zones still retain a record of their protoliths or of subduction processes. Importantly, these samples have been comprehensively characterized for their major-element, trace-element and Sr isotopic compositions as well as for Fe³⁺/ΣFe, from which oxygen fugacity (*f*O₂) is calculated (Aulbach et al., 2022). Oxygen fugacity has been linked to the uptake of H₂O in NAMs in peridotite (e.g., H. Liu & Yang, 2020; Zhang et al., 2022), and the present data set allows a first assessment of the extent to which this observation also applies to eclogite xenoliths. As the OH-dipoles are not aligned to the crystallographic axes and vary with chemical composition, spectra in this study were acquired on oriented crystals in polarized mode. Thus, contributions for the main refractive indices (*α*, *β*, *γ*) could be determined independently, enabling the examination of their relationship with compositional and physical properties. Conversely, although we review the relationships of *c*(H₂O) with various mineral compositional parameters, it is not an aim of this study to constrain the nature of OH defects or by which coupled substitutions it may be incorporated. In addition, electrical conductivities and seismic properties are calculated for samples in this study and from the literature, which may be useful in geophysical studies on the structure and evolution of the cratonic lithosphere. Finally, unless a significant diffusional exchange with surrounding peridotite has occurred (cf. Marshall et al., 2018), the data on relatively pristine eclogite xenoliths, as opposed to those that have been modified during their extended residence in the lithospheric mantle, can be used to estimate the amount of H₂O that has been recycled to the convecting mantle over eons of subduction.

2. Geological Background, Samples, and Prior Work

All samples from the two cratons in this study were previously studied for petrographic characteristics, mineral major and trace element composition (Aulbach et al., 2020; Schmidberger et al., 2007) and Mössbauer-derived Fe³⁺/ΣFe ratios (Aulbach et al., 2019, 2022). Much of the Siberian craton is unconformably overlain by

Phanerozoic sediments and basalts, except on the Aldan and Anabar shields (e.g., Moreira et al., 2023), and underlain by a lithospheric keel that has yielded Paleoproterozoic and Archean ages, as determined for peridotite xenoliths entrained in Devonian and Cretaceous kimberlites (Doucet et al., 2015; Ionov, Carlson, et al., 2015; Ionov, Doucet, et al., 2015; Ionov et al., 2020; Pearson, Shirey, et al., 1995) as well as crustal xenoliths (e.g., Moya et al., 2017) and outcrops (Moreira et al., 2023). Eclogites form part of these xenolith suites, and have been dated to 2.9–2.7 Ga, suggesting emplacement during collision of cratonic nuclei and consumption of intervening ocean basins (Jacob et al., 1994; Pearson, Snyder, et al., 1995). The exceptionally fresh nature of xenoliths in the unserpentinized parts of the Udachnaya East kimberlite pipe has been highlighted (e.g., Ionov et al., 2010; Kamenetsky et al., 2012, 2014; Kitayama et al., 2017). Unsurprisingly, eclogite xenoliths from that locality have been the focus of intense prior study, with interpretations converging on their origin as various parts of subducted oceanic crust (e.g., Agashev et al., 2018; Jacob et al., 1994; Jerde et al., 1993; Kolesnichenko et al., 2018; Mikhailenko et al., 2016, 2021; Mikhailenko, Golovin, et al., 2020; Mikhailenko, Stagno, et al., 2020; Ponomarenko et al., 1980; Radu et al., 2017; Safronov et al., 1980; Snyder et al., 1997; Sobolev, 1977; Spetsius, 1995, 2004). Samples from the Udachnaya-East kimberlite in this study comprise 12 medium- to coarse-grained eclogite xenoliths. Most of them are high-Ca eclogites, some with significant positive Eu anomalies qualifying them as gabbroic eclogites (using the classification of Aulbach and Jacob (2016)) (Figures 1a and 1b). They show LREE-depletions that may reflect partial melt loss (Figure 1c). Because the samples are generally small (5–15 cm longest dimension) and fresh grains were prioritized for Mössbauer analysis, the supply of clear grains for Fourier Transform Infrared Spectroscopy (FTIR) analysis was limited for some of them.

The Slave craton comprises the Hadean to Mesoproterozoic (4.0–2.9 Ga) Central Slave Basement Complex in the western part, and an isotopically juvenile domain (<2.85 to 2.7 Ga) in the eastern part, which were amalgamated at ca. 2.7 to 2.6 Ga (Bleeker, 2002; Davis et al., 2003; Helmstaedt, 2009). Jurassic to Eocene kimberlites (Creaser et al., 2004; Heaman et al., 2004) entrained abundant xenoliths with peridotites of dominantly ~2.8 Ga age, and distinctly younger eclogite (Heaman & Pearson, 2010). The metamorphism of eclogite xenoliths from the central Slave craton has been dated to ca. 1.9 Ga, with a protolith that is older by several 100 Ma, and altogether they are interpreted as reflecting oceanic crust subducted during Paleoproterozoic collision at the western craton margin (Aulbach et al., 2009; Schmidberger et al., 2007). Most eclogite samples have a marked gabbroic signature, and some 20% were overprinted by a kimberlite-like melt at a pressure interval of ~2–5 GPa (Aulbach et al., 2020). This type of metasomatism has led to the formation of high-Mg eclogites or pyroxenites (Smart et al., 2009), which were avoided in this study. Instead, three relatively pristine samples, all gabbroic eclogites with depleted REE patterns, were chosen (Figure 1c), for which enough crush material was available to measure $\text{Fe}^{3+}/\Sigma\text{Fe}$ in garnet and separate minerals for study by FTIR. Table S1 in Supporting Information S1 summarizes salient characteristics for clinopyroxene and garnet in the eclogite xenoliths under study that will be used in various diagrams.

3. Sample Preparation and Analytical Methods

3.1. Fourier Transform Infrared Spectroscopy (FTIR)

In pyroxenes, OH defects form dipoles that usually neither have a clear relation to the crystallographic axes nor to the main refractive indices. Thus, in order to fully characterize OH defects, three orthogonal polarized measurements (e.g., parallel to the main refractive indices) are necessary (Libowitzky & Rossman, 1996). Unpolarized measurements on unoriented crystal sections are less complicated to perform but do not allow conclusions with respect to the dipole orientation. In garnet, due to its cubic symmetry, unpolarized measurements on unoriented sections are sufficient. Here, up to 50 fragments (typically 0.5–1.0 mm across) of clinopyroxene and 10 grains of garnet were picked from crush and prepared as double polished epoxy mounts with thicknesses between 80 and 400 μm . Suitable fragments (i.e., cut perpendicular to the optical axis, or to the obtuse or acute bisectrix) were identified by conoscopic interference figures and used for IR spectroscopy measurements.

Water contents of optically clear parts of clinopyroxene and garnet grains were determined by FTIR at Institut für Mineralogie und Petrographie, Universität Innsbruck (Austria) using a Vertex 70 FTIR spectrometer from Bruker, connected to a Hyperion 3000 microscope equipped with an MCT detector. All spectra were obtained in transmittance mode, using non-polarized IR radiation for garnet and polarized IR radiation for oriented clinopyroxene, mostly using a square aperture of 50 \times 50 μm (aperture was occasionally adjusted to avoid impurities). Each acquired spectrum was scrutinized for irregularities. On average, 40%–50% of the spectra (Figure S1 in

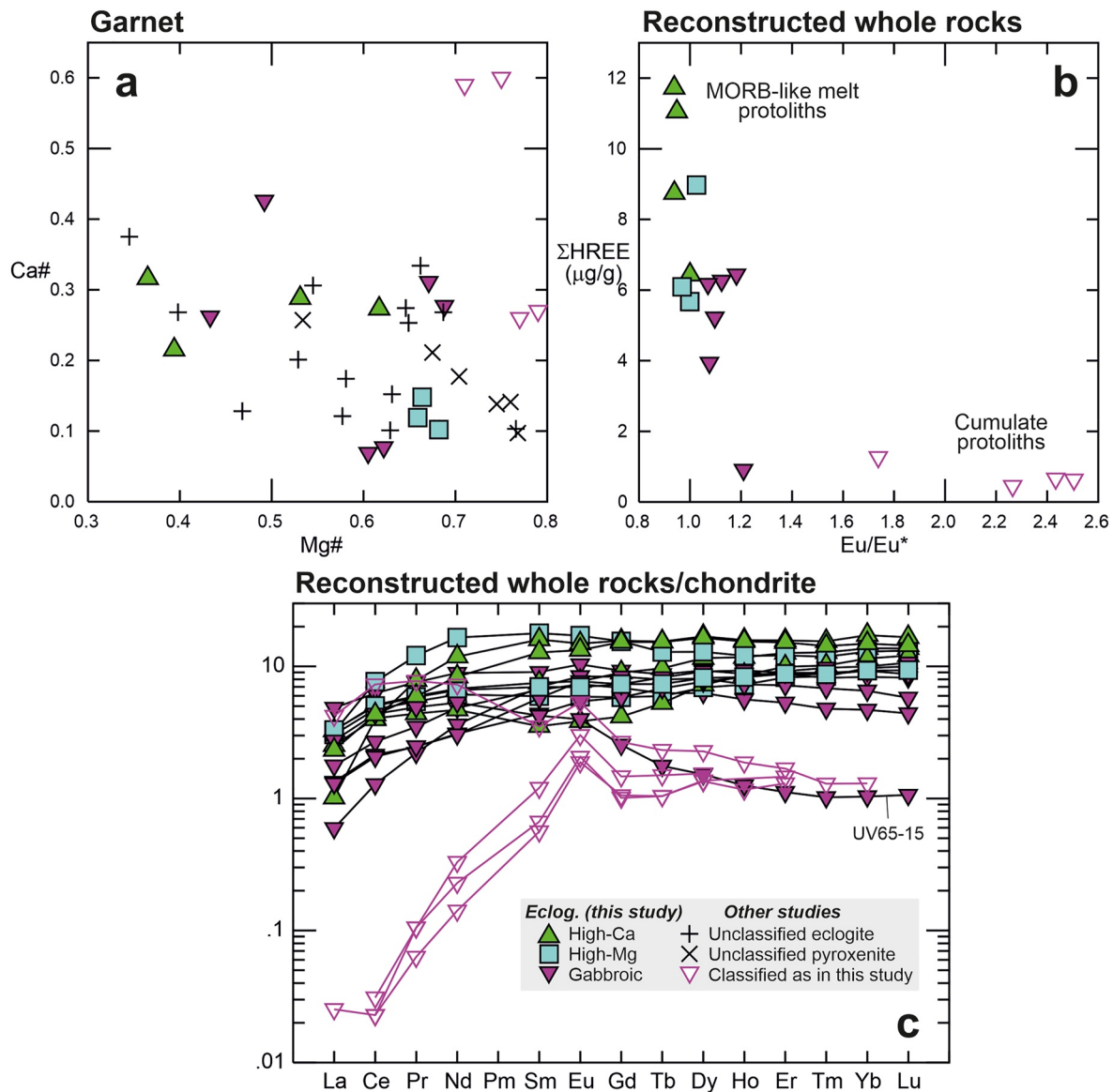


Figure 1. Garnet and reconstructed bulk-rock compositions of eclogite and pyroxenite xenoliths (classified according to Aulbach and Jacob (2016)) from the Siberian and Slave cratons. (a) Ca# ($\text{Ca}/(\text{Ca} + \text{Mg} + \text{Fe}^{\text{total}} + \text{Mn})$) versus Mg# ($\text{Mg}/(\text{Mg} + \text{Fe}^{\text{total}})$) in garnet; (b) ΣHREE ($\mu\text{g/g}$) as a function of the size of the Eu anomaly ($\text{Eu}/\text{Eu}^* = \text{chondrite-normalized Eu}/(\text{Sm} \cdot \text{Gd})^{0.5} > 1.05$; Rudnick & Fountain, 1995) in reconstructed whole rocks, allowing the identification of eclogite xenoliths with suggested plagioclase-rich cumulate versus residual MORB-like melt protoliths (Aulbach & Jacob, 2016); the four samples with the highest Eu/Eu^* are from Obnazhennaya; (c) chondrite-normalized REE patterns (chondrite of McDonough and Sun (1995)). Samples in this study are shown with filled symbols, literature data (Koch-Müller et al., 2004; Kolesnichenko et al., 2018; Matsyuk et al., 1998; Radu et al., 2022; Snyder et al., 1995; Taylor et al., 2016) with reported H_2O abundances (all from the Siberian craton) are shown with open symbols and crosses (“unclassified” refers to the lack of trace-element information required for classification).

Supporting Information S1) exhibited features that were interpreted as interferences from other, optically invisible phases, such as increased absorption between the main absorption bands related to OH, leading to weaker separation than in regular spectra, increased absorption beyond the main OH bands (“shoulders”) mainly in the wavenumber range $3,300\text{--}3,000\text{ cm}^{-1}$, or sharp bands near wavenumber $3,700\text{ cm}^{-1}$ (Figure S2 in Supporting Information S1). The respective spectra were not considered for the quantification of structural OH in pyroxene (see Text S1 in Supporting Information S1). In contrast, the OH contribution by solid inclusions of NAMs, such as rutile and quartz in four samples (Figure S3 in Supporting Information S1), is considered insignificant (Text S1 in Supporting Information S1). Greatly variable absorptions at wavenumbers $3,624\text{--}3,600\text{ cm}^{-1}$ have previously been observed in omphacite from Siberian eclogite xenoliths (Koch-Müller et al., 2004), which was interpreted to reflect sub-microscopic inclusions of hydrous minerals. In the present study, water concentrations are relatively

homogeneous, even in samples where this band dominates (e.g., UV5-14 and MX121), whereas we would expect greater variability related to random inclusions. In the present study, we consider this band to reflect structural OH because its absorbance shows a very low variability (on average 9% for the α component within one grain; Table S5).

Integrated absorbances were converted into water contents (in wt.ppm) via the modified Beer-Lambert law ($c(\text{H}_2\text{O}) = A_{\text{tot}}/\epsilon \times \rho \times t$), with integrated absorbance A_{tot} , the specific absorption coefficient ϵ , density ρ , and plate thickness t . The absorption coefficients of Bell et al. (1995) were used, which is the calibration used in most previous studies on eclogite xenoliths, allowing for direct comparison, although we note that typically lower concentrations are obtained using the calibration of Libowitzky and Rossman (1997) (Text S1 in Supporting Information S1). Water contents for clinopyroxene in each sample were calculated by adding the averages of the three contributions (α , β , γ ; Libowitzky & Rossman, 1997) for polarized measurements or multiplied by three for unpolarized clinopyroxene measurements (Kovács et al., 2008), which were acquired for selected samples for comparison (Text S1 in Supporting Information S1). Results for $c(\text{H}_2\text{O})$ along the refractive indices α , β , and γ in omphacite as well as total contents for both omphacite and garnet are reported in Table 1. Concentrations for α and β were found to be indistinguishable, as in previous studies (Agasheva et al., 2021; Koch-Müller et al., 2004; Kolesnichenko et al., 2018; Radu et al., 2022).

Combined uncertainties in $c(\text{H}_2\text{O})$ related to baseline correction, experimentally determined extinction coefficients and thickness (determined 1–3 times per grain with an average uncertainty of 1.5 μm per 100 μm thickness; Tables S2–S4 in Supporting Information S1), as well as contributions from undetected contamination and non-ideal orientation of some grains, are estimated to be $\sim 20\%$, while the detection limit is estimated to be ~ 2 ppm. This is similar to the average relative uncertainty for $c(\text{H}_2\text{O})$ ($\sim 15\%$) when considering the standard deviations given in Table S5. The average relative standard deviation for α and γ for multiple spectra obtained on the same grain is 7%, which suggests limited effects of diffusive H_2O loss or gain at the fragment scale. Further details regarding sample preparation, data acquisition and reduction, quantification of H_2O abundances and the effects of (sub)microscopic inclusions are provided in Text S1 in Supporting Information S1.

3.2. Secondary Ion Mass Spectrometry (SIMS)

Garnet grains in eclogite xenoliths from Udachnaya were embedded in an epoxy plug and analyzed by Secondary Ion Mass Spectrometry (SIMS) at the Canadian Centre for Isotopic Microanalysis (CCIM), University of Alberta, as previously described for samples from Diavik investigated in this study, for which oxygen isotope compositions (denoted as $\delta^{18}\text{O}_{\text{VSMOW}}$, i.e., the ‰ deviation from the VSMOW standard) have been previously reported (Aulbach et al., 2019). In brief, garnet mineral fragments were mounted with CCIM garnet reference materials S0068 (Gore Mountain Ca-Mg-Fe garnet) and S0088B (grossularite), exposed in a 25 mm diameter epoxy assembly (M1506) using diamond grits and characterized by scanning electron microscopy. Subsequently, oxygen isotope ratios were determined with a Cameca IMS 1280 multicollector ion microprobe using a $^{133}\text{Cs}^+$ primary beam, with an impact energy of 20 keV, beam current of ~ 2.0 – 2.5 nA, probe diameter of ~ 12 μm , and simultaneous detection of oxygen ions in Faraday cups. Reference materials S0068 (UAG) and S0088B ($\delta^{18}\text{O}_{\text{VSMOW}} = +5.72$ and $+4.13$, respectively) were analyzed repeatedly, whereby data for S0088B and unknowns were first corrected for instrumental mass fractionation (IMF) to S0068 garnet, and then further corrected according to their Ca# ($\text{Ca}/[\text{Ca} + \text{Mg} + \text{Fe}]$), as determined by electron microprobe. The 95% confidence uncertainty on $\delta^{18}\text{O}_{\text{VSMOW}}$ in garnet, including errors relating to within-spot counting statistics, geometric effects, correction for IMF, and matrix effects relating to Ca# is estimated to be $\pm 0.30\%$. Further details are provided in Ickert and Stern (2013). While slightly different correction themes do exist (e.g., Martin et al., 2014), the veracity of the current scheme for eclogitic garnets has been validated in a recent study reporting SIMS data using the calibration method adopted for this paper and obtained from bulk laser fluorination, and the two are in excellent agreement (Hardman et al., 2021).

4. Results and Comparison to Prior Studies on Eclogite Xenoliths From the Siberian Craton

4.1. Spectral Features Related to Lattice Overtones and to OH

Polarized IR spectra for clinopyroxene show distinct features in the range of the lattice overtones (wavenumber range $\sim 2,300$ – $1,350$ cm^{-1}) depending on the orientation, which can be exploited to identify the orientation

Table 1
Water Contents, Garnet $\delta^{18}\text{O}$ and Physical Properties of Eclogite Xenoliths From Udachnaya (UV...), Siberian Craton and Diavik, Slave Craton (MX...)

Sample	Clinopyroxene				Garnet			Reconstructed WR H_2O^a	
	$\alpha\text{-H}_2\text{O}$ (wt.ppm)	$\gamma\text{-H}_2\text{O}$ (wt.ppm)	$\text{H}_2\text{O}_{\text{cpx}}$ total (wt.ppm)	$\delta^{18}\text{O}$ (‰)	$\text{H}_2\text{O}_{\text{gt}}$ (wt.ppm)	From meas. mineral conc.	Hypo. equil. (w/kimberlite)		
MX121	G	138	153	423	5.15	195	298	258	
MX133	G	49	133	229	6.03	<dl	104	241	
MX45 ^b	G	138	192	(512 max)	5.84	(441 max)	na	na	
UV114-11	HMg	119	101	339	5.81	25	166	257	
UV121-14	HCa	86	84	296	5.94	69	171	217	
UV16-15	HMg	47	62	150	5.88	2	69	245	
UV192-11	HMg	89	83	272	6.12	12	129	273	
UV5-14	HCa	35	33	103	7.07	<dl	47	300	
UV568A-10	HCa	125	125	374	6.76	6	172	286	
UV59-2017	G	65	209	339	7.25	<dl	153	312	
UV64-12	G	71	206	348	6.80	23	169	248	
UV64-14	G	49	65	156	5.54	34	89	263	
UV65-15	G	147	88	362	4.99	57	194	267	
UV79-14	HCa	35	89	166	7.32	<dl	75	236	

$D(\text{H}_2\text{O})$	Pressure-temperature-depth		
	$\Delta\log f\text{O}_2$ (FMQ)	$T_{\text{KR88}}@P_{\text{HCl1}}$ (°C)	$P_{\text{HCl1}}@T_{\text{KR88}}$ (GPa)
cpx-gt			
MX121	-2.36	1098	5.2
MX133	-4.67	662	3.1
MX45 ^b	-4.38	657	3.0
UV114-11	-4.11	976	5.4
UV121-14	-1.40	992	5.5
UV16-15	-3.77	883	4.7
UV192-11	-5.03	1021	4.7
UV5-14	-2.82	830	4.3
UV568A-10	-2.45	850	4.4
UV59-2017	-5.93	840	4.3
UV64-12	-2.67	821	4.2
UV64-14	-2.34	895	4.8
UV65-15	-3.32	1063	5.0
UV79-14	-2.44	742	3.6

Table 1
Continued

	Density-seismic velocity ^d			Electrical conductivity ^e		
	rho (g/cm ³)	Vp (km/s)	Vs (km/s)	Dry gt/wet cpx (Log S/m)	Wet gt/wet cpx (Log S/m)	Wet gt/wet cpx (Log S/m)
MX121	3.59	8.53	4.80	-2.38	-1.63	-1.00
MX133	3.63	8.49	4.80	-4.65	-4.74	-3.75
MX45				na	na	na
UV114-11	3.62	8.62	4.86	-2.93	-2.58	-1.84
UV121-14	3.64	8.46	4.78	-2.89	-2.26	-1.61
UV16-15	3.66	8.54	4.84	-3.45	-3.68	-2.87
UV192-11	3.57	8.57	4.84	-3.76	-4.05	-3.22
UV5-14	3.57	8.56	4.84	-3.46	-3.40	-2.50
UV568A-10	3.61	8.52	4.79	-3.53	-3.78	-2.89
UV59-2017	3.64	8.53	4.82	-3.62	-3.15	-2.35
UV64-12	3.55	8.66	4.90	-3.39	-2.88	-2.22
UV64-14	3.54	8.71	4.94	-2.73	-2.69	-1.92
UV65-15	3.53	8.76	5.00	-2.53	-2.09	-1.41
UV79-14	3.53	8.74	4.99	-4.18	-4.37	-3.45

Note. G—gabbroic, HMg—high-Mg, and HCa—high-Ca (classification of Aulbach and Jacob (2016)); α and γ refer to polarization during FTIR measurement; cpx—clinopyroxene, gt—garnet, and dl—detection limit (estimated at 2 wt ppm); WR—whole rock; $\delta^{18}\text{O}$ —‰ deviation from the VSMOW standard; and D —distribution coefficient, where numbers in parentheses were calculated with 1.4 ppm in garnet when no H₂O was detected (see text); FMQ—relative to the Fayalite-Magnetite-Quartz buffer, oxybarometer of Stagno et al. (2015); Vp and Vs—compressional and shear wave velocity, respectively.

^aReconstructed for mineral modes of 0.55 garnet + 0.45 clinopyroxene (see text) and measured H₂O concentrations (conc.) in the minerals and for hypothetical (hypoc.) H₂O concentrations in clinopyroxene and garnet in equilibrium (equib.) with a kimberlite containing 3 wt % H₂O, using mineral-melt distribution coefficients as a function of Al₂O₃ in clinopyroxene and TiO₂ in garnet and the relationships reported in Aulbach et al. (2008). ^bUnclean spectra, maximum H₂O values. ^cData in Aulbach et al. (2022). KR88 refers to the geothermometer of Krogh (1988), HCl1 to the relevant geothermal gradient parameterized from Hasterok and Chapman (2011) (see Text S1 in Supporting Information S1 for details). ^dTaken from the spreadsheet of Abers and Hacker (2016) at the preferred pressures and temperatures; average uncertainty related to T (60°C) and P (1 GPa) uncertainty (see text) is 0.019 g/cm³ for rho, 0.046 km/s for Vp and 0.012 km/s for Vs. ^eWet and dry gt calculated at P and T after Dai and Karato (2009), wet cpx after Zhao and Yoshino (2016), wet gt and wet cpx after H. Liu et al. (2019); average uncertainty related to T (60°C) and P (1 GPa) uncertainty (see text) is 10^{0.24}, 10^{0.22}, and 10^{0.20} S/m, respectively, for electrical conductivity.

independently of the optical microscope (cf. Stalder & Ludwig, 2007). This step allows us to check the assignment of the polarized spectra to a vibration direction. Spectra for polarization parallel to α and γ show two major bands at wavenumbers $\sim 2,000$ – $1,900$, $\sim 1,750$ – $1,500$ cm^{-1} , whereby the band at lower wavenumber is broadly tripartite (Figure 2). While the absorbance for the γ bands at those two wavenumber intervals almost always increases with decreasing wavenumber, the absorbance ratio for bands in α is more variable, with the strongest absorption near $\sim 1,750$ – $1,700$ cm^{-1} . Polarization parallel to β results in spectra characterized by three bands that are shifted relatively to α and γ , whereby a broad flat-topped band at $\sim 2,100$ – $1,950$ cm^{-1} is characteristic, the other bands having higher and subequal absorbance at $\sim 1,650$ – $1,550$ and $\sim 1,450$ – $1,350$ cm^{-1} (Figure 2).

Absorption bands related to lattice overtones



Figure 2. Typical Fourier Transform Infrared Spectroscopy absorption bands related to lattice overtones for clinopyroxene in four eclogite xenoliths from the Siberian and Slave cratons.

The main OH absorption bands in omphacite occur at wavenumbers I \sim 3,630–3,600, II 3,530–3,510, and III 3,470–3,430 cm^{-1} (Huang et al., 2014; Koch-Müller et al., 2004; Libowitzky & Beran, 2006). The dominant band for γ is always at band III, but absorbance varies between narrow sharp bands at III with bands $\gg \alpha$ or β and no absorbance at band I to intensity similar to α and β and some absorbance at band II (Figure 3). Both band I and III are always recognized for α and β , whereby the intensity at band III may be $>I$ or vice versa. These features are interpreted to relate to the structural environment and clinopyroxene compositions, as strong Type III bands prominent for γ have been linked to jadeite-rich clinopyroxene, whereas strong Type I bands prominent for α (and β) relate to diopside-rich clinopyroxene (Smyth et al., 1991). In contrast, broad shoulders overlapping type III bands are considered to be associated with contamination and therefore rejected (examples in Figure 4).

4.2. Water Concentrations in Clinopyroxene, Garnet, and Reconstructed Whole Rocks, With Comparison to Prior Work

OH absorption contributions (recalculated as water contents) in clinopyroxene from Udachnaya eclogite xenoliths determined in polarized mode range from 35 to 150 wt.ppm for the α -polarized component, and from 33 to 210 wt.ppm for the γ -polarized component, with calculated total clinopyroxene $c(\text{H}_2\text{O})$ ranging from 100 to 510 wt.ppm (Table 1). The α -polarized component in clinopyroxene in the two samples from Diavik has $c(\text{H}_2\text{O})$ of 50 and 140 wt.ppm, while the γ -polarized component has $c(\text{H}_2\text{O})$ of 130 and 150 wt.ppm, corresponding to a total $c(\text{H}_2\text{O})$ of 230 and 420 wt.ppm, respectively. The OH contribution for the two components is very weakly correlated at best (Figure 5a). In the samples investigated, total clinopyroxene $c(\text{H}_2\text{O})$ obtained by polarized measurements on oriented crystals (Figure 5b) agrees within uncertainty with that derived from unpolarized measurements in unoriented grains (Table S5), as previously demonstrated by Radu et al. (2022). For comparison, Koch-Müller et al. (2004) report 60–890 wt.ppm H_2O (calibration of Bell et al. (1995)) for omphacite in eight eclogite xenoliths from various Siberian localities, which are minima because the authors did not consider Type III bands in their totals, ascribing them entirely to contamination. Kolesnichenko et al. (2018) present results for omphacite in 19 samples from Udachnaya with $c(\text{H}_2\text{O})$ from below detection to 100 wt.ppm, while Radu et al. (2022) report 870–1,320 wt.ppm H_2O in clinopyroxene from four eclogite xenoliths from Obnazhenaya (northeast of Udachnaya), which are characterized by unusual exsolution features including zoisite lamellae.

Water contents in garnet from Udachnaya eclogites range from below detection ($n = 3$) to 70 wt.ppm, and $c(\text{H}_2\text{O})$ in the two samples from Diavik is below detection and 200 wt.ppm, respectively (Table 1; Figure 5c; garnet and clinopyroxene in a third sample are affected by submicroscopic inclusions; Text S1 in Supporting Information S1). Snyder et al. (1995) and Matsyuk et al. (1998) report $c(\text{H}_2\text{O})$ for garnet in 28 samples from Udachnaya and other localities, with concentrations of below detection to 98 wt.ppm (average 27 wt.ppm), while $c(\text{H}_2\text{O})$ garnet in the study of Kolesnichenko et al. (2018) is below detection. Here, when the water content in the garnet is below the limit of detection (~ 2 wt.ppm), its $c(\text{H}_2\text{O})$ is estimated to be 1.4 wt.ppm H_2O , which is derived as the limit of detection $\times \sqrt{2}/2$ and designed to avoid biasing the database toward high values (Antweiler, 2015). This content is used for the purpose of plotting, and of reconstructing bulk-rock chemical compositions and conductivities.

Bulk rock $c(\text{H}_2\text{O})$ were reconstructed from clinopyroxene and garnet using modal abundances of 45 and 55 wt.% respectively, with an estimated uncertainty of 10%. This is done because the combination of medium to coarse grain size in eclogite xenoliths, with hand specimens rarely exceeding 5 cm, precludes accurate determination of mineral modal abundances at the section scale. The proportion and uncertainty used here are considered reasonable because a suite of unique large (1–20 kg) eclogite xenoliths from Udachnaya yields average modal abundances of 55.4 ± 5.1 (1 σ ; $n = 17$) wt% for garnet and 44.3 ± 5.0 wt% for clinopyroxene (Agashev et al., 2018) (see further rationalization in Aulbach and Jacob (2016) and Aulbach et al. (2020)). Reconstructed bulk rocks have $c(\text{H}_2\text{O})$ from 50 to 190 wt.ppm for samples from Udachnaya, and 100 and 300 wt.ppm H_2O , respectively, for the two samples from Diavik (Table 1). The uncertainty on H_2O content in reconstructed bulk rocks, arising from $\sim 10\%$ uncertainty in modal abundances (e.g., Aulbach et al., 2020) and from the estimated 20% on mineral H_2O abundances, is estimated conservatively at 30%. Rutile is present in thick sections of six of the Udachnaya samples studied here (Aulbach et al., 2022) and was retrieved from crushed material in the two eclogite xenoliths from Diavik (pers. observation). Its modal abundance is estimated (see Aulbach (2020), for procedure) at zero to ~ 1 wt.% (average 0.33 wt.%), and although in eclogite it has reported $c(\text{H}_2\text{O})$ up to 800 wt.ppm (Hammer & Beran, 1991; Katayama et al., 2006), its possible contribution of few wt.ppm to the bulk rock concentration is considered negligible.

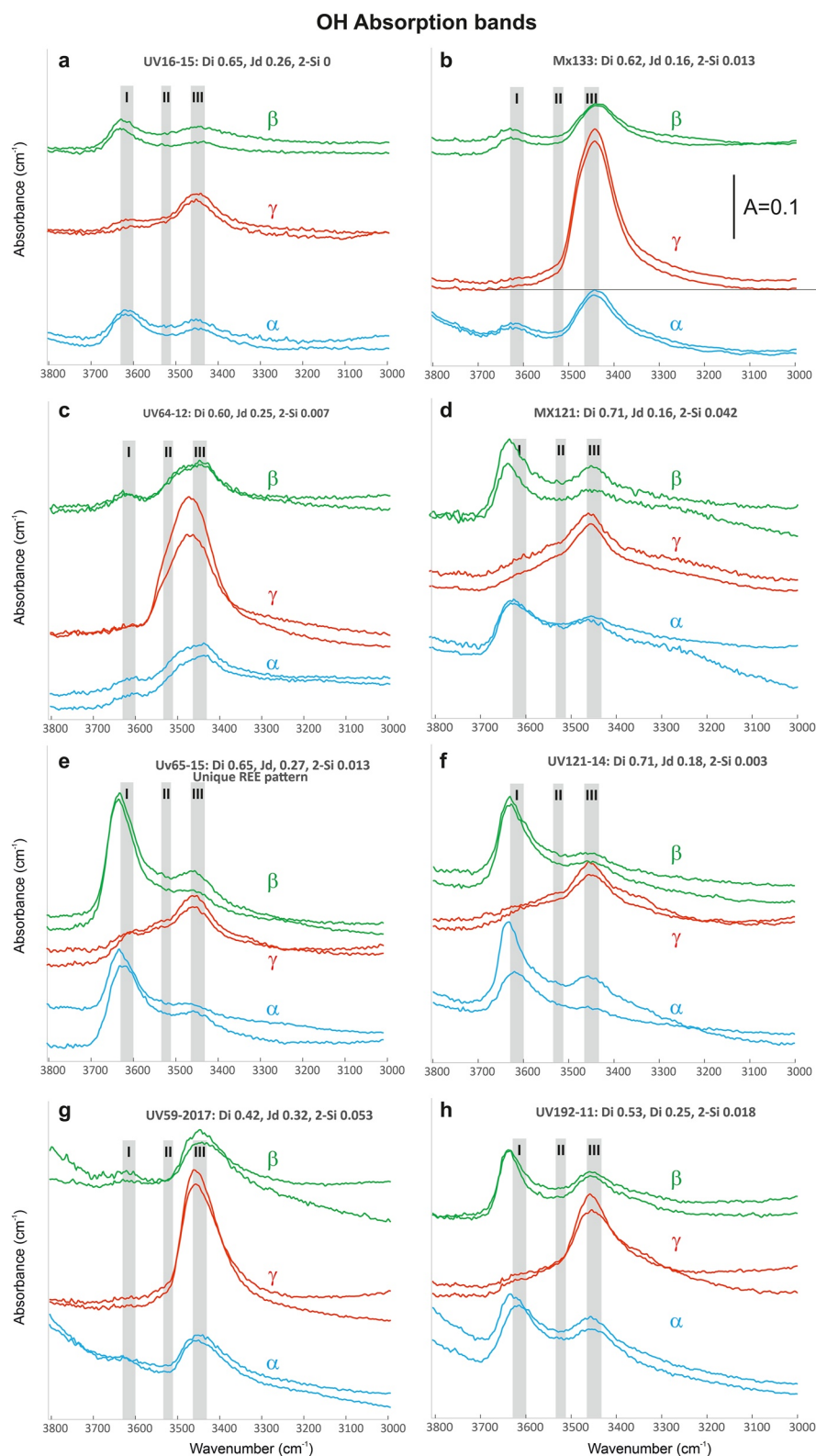


Figure 3. Typical Fourier Transform Infrared Spectroscopy OH absorption bands for clinopyroxene in eight representative eclogite xenoliths from the Siberian and Slave cratons, for polarization parallel to α (blue), β (green), and γ (red), illustrating the similarity of α and β ; spectra are vertically offset for graphical reasons; for absolute values of absorbance (A), see scale bar in panel (b) Diopside (Di) and jadeite (Jd) components are given as well as 2-Si cations per formula unit (Table S1 in Supporting Information S1) reflecting the degree of silica-deficiency.

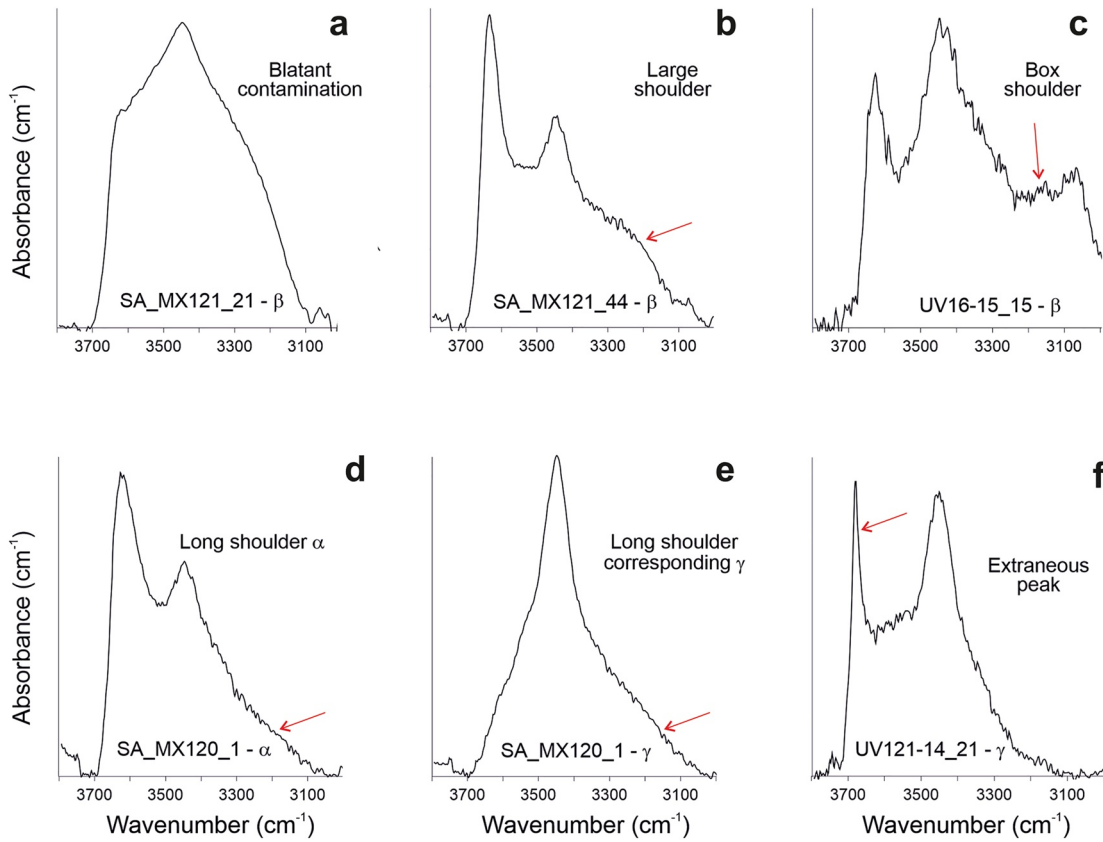


Figure 4. Typical Fourier Transform Infrared Spectroscopy OH absorption bands showing various features (red arrows) associated with contamination, entailing rejection (see also Figure S1 in Supporting Information S1 for accepted vs. rejected spectra for all analyses in two representative samples, and Figure S2 in Supporting Information S1 for the full range of features).

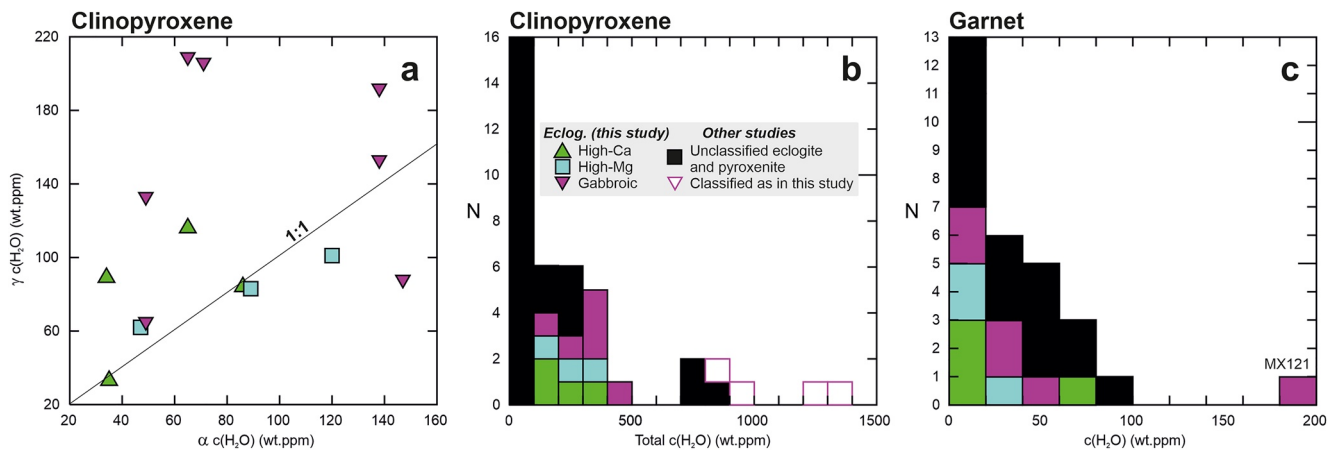


Figure 5. H₂O concentrations for two polarized components in clinopyroxene and bulk H₂O concentrations in clinopyroxene and garnet from various classes of eclogite and pyroxenite xenoliths from the Siberian and Slave cratons. (a) H₂O concentration of the γ -polarized component as a function of the α -polarized component in clinopyroxene. Total H₂O concentrations in (b) clinopyroxene and (c) garnet. References for other studies as in Figure 1, “unclassified” refers to the lack of trace-element information required for classification.

4.3. Oxygen Isotope Compositions

For the garnet in samples from Udachnaya, $\delta^{18}\text{O}$ ranges from +4.99 in a gabbroic eclogite (UV65-15) to +7.32‰ in a high-Ca eclogite (UV79-14), whereby gabbroic eclogites span nearly the entire range of $\delta^{18}\text{O}$, whereas three high-Mg eclogites show a narrow $\delta^{18}\text{O}$ range of 5.81–6.12 (Table 1). For comparison, the two previously investigated samples from Diavik have $\delta^{18}\text{O}$ of 5.15 and 6.03 (Aulbach et al., 2019).

5. Estimates of Physical Properties (Pressure, Temperature, Density, Seismic Velocity, and Electrical Conductivity)

In keeping with Aulbach et al. (2020), garnet-clinopyroxene Mg-Fe exchange temperatures (formulation of Krogh (1988); T_{KR88}) are calculated iteratively with parameterizations of steady-state conductive geotherms of Hasterok and Chapman (2011, HC11), which are determined regionally based on peridotite xenoliths or xenocrysts for which reliable geobarometers have been calibrated (e.g., Nimis & Grütter, 2010). These estimates are subject to uncertainties due to advective heating identified in some of the samples, with temperature-pressure uncertainties estimated at 60°C and 1 GPa, respectively (Text S1 in Supporting Information S1). Densities (3.56–3.66 g/cm³) and seismic P-wave velocities V_p (8.44–8.62 km/s) at preferred P - T (reflecting the eclogite xenoliths' position in the lithospheric mantle prior to entrainment; Table 1) were taken from the spreadsheet of Abers and Hacker (2016). Using Hashin-Shtrikman lower (HS−) and upper (HS+) bounds (formulations in Jones et al., 2009), electrical conductivity ($10^{-4.7}$ – $10^{-2.4}$ S/m) was calculated based on the temperature- H_2O -conductivity relationship for diopside-rich wet clinopyroxene in Zhao and Yoshino (2016), combined with the relationship for dry pyrope-rich garnet in Dai and Karato (2009) considered most appropriate in terms of calibrated range. All calculated physical parameters and uncertainty estimates are reported in Table 1 (see also footnote therein), and more details are provided in Text S1 in Supporting Information S1.

6. Discussion

6.1. Influence of Temperature and $\text{Fe}^{3+}/\Sigma\text{Fe}$ on OH Dipole Orientation in Eclogitic Clinopyroxene

Hydrogen is incorporated in NAMs via various lattice defect types and is therefore dependent on mineral composition and pressure-temperature in addition to water fugacity ($f\text{H}_2\text{O}$) and oxygen fugacity ($f\text{O}_2$) (e.g., Demouchy & Bolfan-Casanova, 2016; Peslier et al., 2017). Several studies have delineated the crystal-chemical controls on OH incorporation in garnet and pyroxenes, which are complex due to extensive solid solutions and multiplicity of hydrogen-associated point defects (e.g., Ingrin & Skogby, 2000; Lu & Keppler, 1997; Mookherjee & Karato, 2010; Reynes et al., 2020; Stalder, 2004; Stalder & Ludwig, 2007). As contributions for polarization parallel to α and β are indistinguishable (Agasheva et al., 2021; Koch-Müller et al., 2004; Kolesnichenko et al., 2018; Radu et al., 2022; this study), the orientation of the OH dipole is reflected by the ratio of γ to α component.

In this study, there is no correlation of the Ca-Eskola component (M2 site vacancies calculated as 4 minus the sum of cations; Koch-Müller et al., 2004), which was previously linked to one band in clinopyroxene (Smyth et al., 1991), with the ratio of γ -over α -polarized component ($r^2 = 0$; compare Table 1, Table S1 in Supporting Information S1). There is also no correlation of the γ/α ratio with the jadeite component ($r^2 = 0.05$), but a weak anticorrelation with the diopside component is apparent ($r^2 = 0.20$) (Figure 6a). In contrast, marked correlations between the γ/α ratio and trace elements are observed, specifically a positive one for two monovalent elements (Li and Ag) and a negative one for the high field-strength element Nb (Figures 6b–6d). This may reflect the association of these trace elements with particular crystal lattice sites in clinopyroxene that also affect the dipole orientation. Moreover, the highest γ/α ratios are observed at low $\text{Fe}^{3+}/\Sigma\text{Fe}$ (Figure 7a) and low temperatures (Figure 7b), whereas there is no relationship with $f\text{O}_2$ ($r^2 = 0$). Moreover, $\text{Fe}^{3+}/\Sigma\text{Fe}$ in cpx is positively correlated with temperature in this data set (Figure 7c). As the highest Li and Ag, and the lowest Nb abundances are similarly observed at low temperature (not shown), a temperature-dependence of dipole orientation—and therefore of OH distribution amongst lattice defects—is suggested that is related to a change in the crystal-chemical environment that affects H_2O similarly to (other) incompatible components including Fe^{3+} . Therefore, clinopyroxene γ/α ratio may serve as a rough proxy for temperature or clinopyroxene $\text{Fe}^{3+}/\Sigma\text{Fe}$.

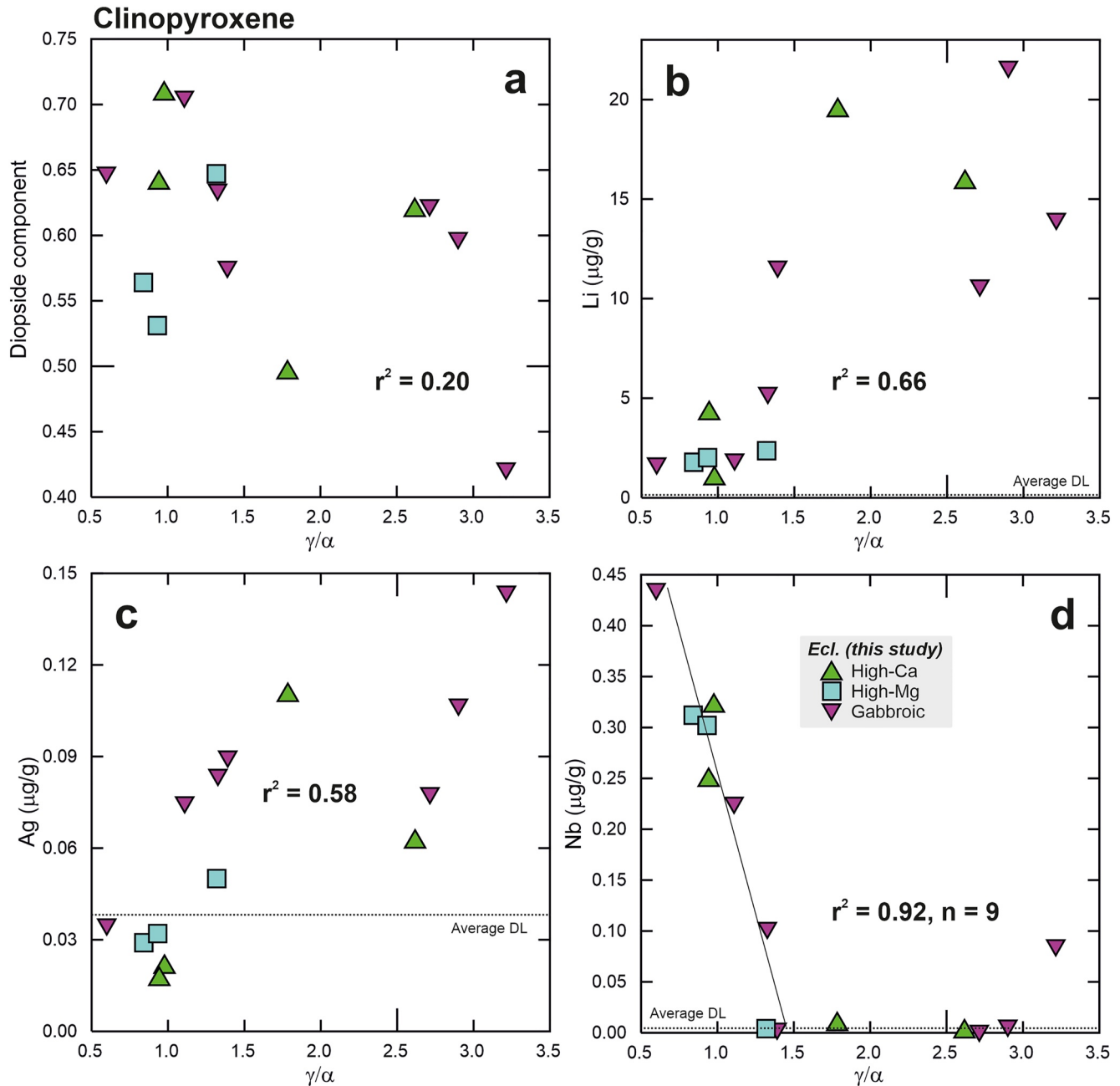


Figure 6. Ratio of γ -over α -polarized component in clinopyroxene as a measure of dipole orientation in eclogite xenoliths from the Siberian and Slave cratons. (a) Diopside component shows no significant covariation, whereas (b) Li, (c) Ag, and (d) Nb abundance shows some correlation that may reflect their association with particular crystal lattice sites in clinopyroxene that also affect dipole orientation. The average detection limits for Li, Ag, and Nb in clinopyroxene were 0.13, 0.039, and 0.004 $\mu\text{g/g}$, respectively (Aulbach et al., 2022).

6.2. T - X - $f\text{O}_2$ Controls on H_2O Incorporation in Omphacite and Garnet

In Si-deficient omphacite from the Siberian craton (Koch-Müller et al., 2004; Kolesnichenko et al., 2018; this study), Al_2O_3 content and tetrahedral Al (calculated as 2-Si cations per formula unit based on 6[O]) are correlated with total water content (Figure 8a). This relationship mirrors the experimentally-determined partitioning of H_2O between clinopyroxene and hydrous andesite melt (Aubaud et al., 2008), which also increases with increasing clinopyroxene Al_2O_3 . Samples with silica-deficient clinopyroxene are further characterized by high Eu/Eu^* (inset in a), qualifying them as gabbroic eclogites with plagioclase-rich, aluminous cumulate protoliths.

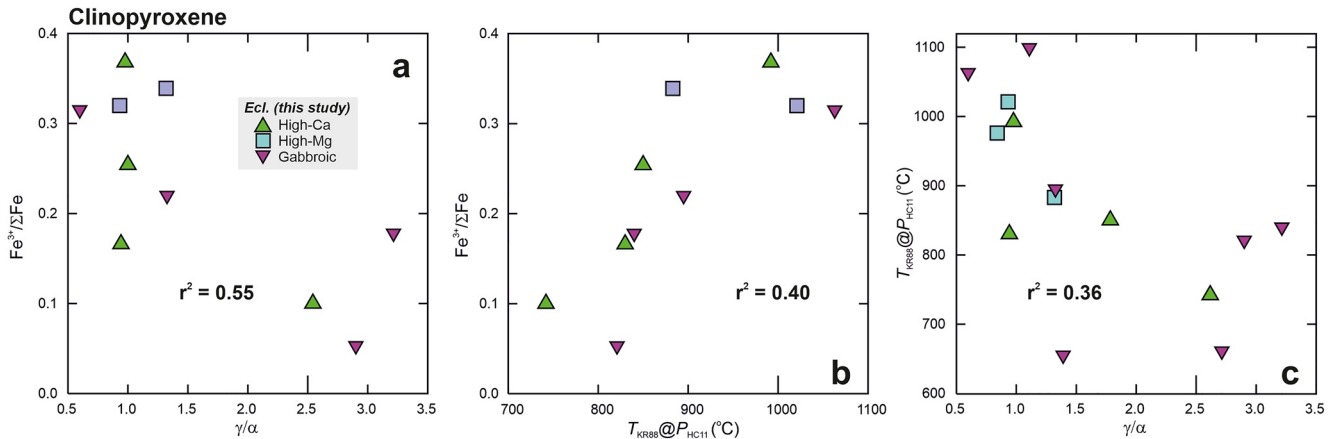


Figure 7. Ratio of γ -over α -polarized component in clinopyroxene in eclogite xenoliths from the Siberian and Slave cratons. (a) High γ/α is linked to low $\text{Fe}^{3+}/\Sigma\text{Fe}$ (with an absolute uncertainty of ~ 0.01 – 0.02), which is itself tied to (b) temperature. Consequently, γ/α is also linked to (c) temperature.

Garnet $c(\text{H}_2\text{O})$ shows no relationship with any major element or component, such as grossular content (i.e., Ca#, Figure 8b), although the garnet in Ti-rich sample MX121 has by far the highest $c(\text{H}_2\text{O})$ (Figure 8c), as also observed for garnet in orogenic eclogite (Gose & Schmädicke, 2018). While this agrees with the suggestion that coupled substitution of 2 Ti on the octahedral site is compensated by 2 H on a Si-site (Reynes et al., 2020), there is no overall relationship for samples in this or prior xenolith studies. In contrast, high garnet $c(\text{H}_2\text{O})$ may be associated with low Li (Figure 9a), and high Nb (Figure 9b), LREE (e.g., La, $r^2 = 0.53$ for garnet in 12 Udachnaya eclogites, Figure 9c) and U abundances (Figure 9d). Lanthanum also shows a positive co-variation with garnet Ca# (inset Figure 9c), which is known to facilitate the partitioning of incompatible elements into garnet from clinopyroxene via the effect of CaO on the geometry of cation sites (e.g., Harte & Kirkley, 1997; O'Reilly & Griffin, 1995). Although garnet Ca# is not clearly related to its H_2O content in this study, a crystal-chemical effect related to the grossular component is expected to contribute to H_2O uptake in garnet, and high Ca was linked to high H_2O in garnet from orogenic eclogite (Gose & Schmädicke, 2018).

Although the highest clinopyroxene $c(\text{H}_2\text{O})$ is observed for the sample with the highest temperature of residence in the continental lithosphere (MX121), consistent with experimental findings of H. Liu and Yang (2020), there is no general relationship of temperature with clinopyroxene $c(\text{H}_2\text{O})$, in contrast to garnet (Figures 10a and 10b).

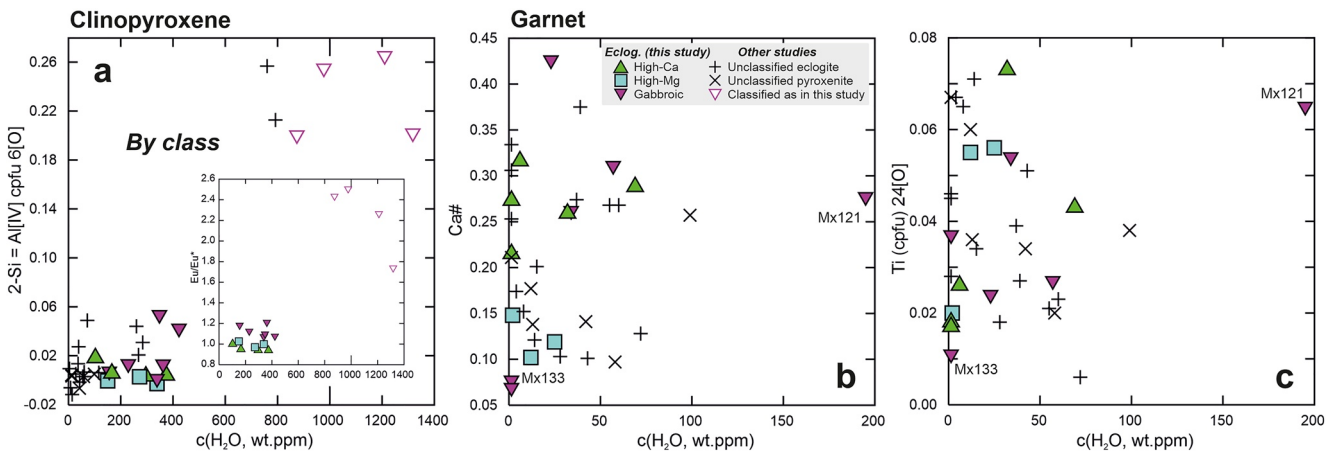


Figure 8. Bulk clinopyroxene and garnet H_2O content (estimated uncertainty 20%) in eclogite and pyroxenite xenoliths from the Siberian and Slave cratons. (a) Bulk clinopyroxene $c(\text{H}_2\text{O})$ versus fraction of tetrahedral Al (Al[IV]) calculated as 2-Si cations per formula unit (cpfu), which is correlated with (inset) Eu/Eu^* (chondrite-normalized $\text{Eu}/(\text{Sm}^*\text{Gd})^{0.5}$; Rudnick & Fountain, 1995) (by eclogite class). Garnet $c(\text{H}_2\text{O})$ is not or is weakly related to (b) Ca# ($\text{Ca}/(\text{Ca} + \text{Mg} + \text{Fe}^{\text{total}} + \text{Mn})$), which is known to facilitate the incorporation of some incompatible trace elements (Harte & Kirkley, 1997; O'Reilly & Griffin, 1995) or to (d) Ti cpfu, which is known to increase H_2O partitioning into experimental garnet in equilibrium with hydrous andesite melt (Aubaud et al., 2008). Data from other studies are shown in Figure 1.

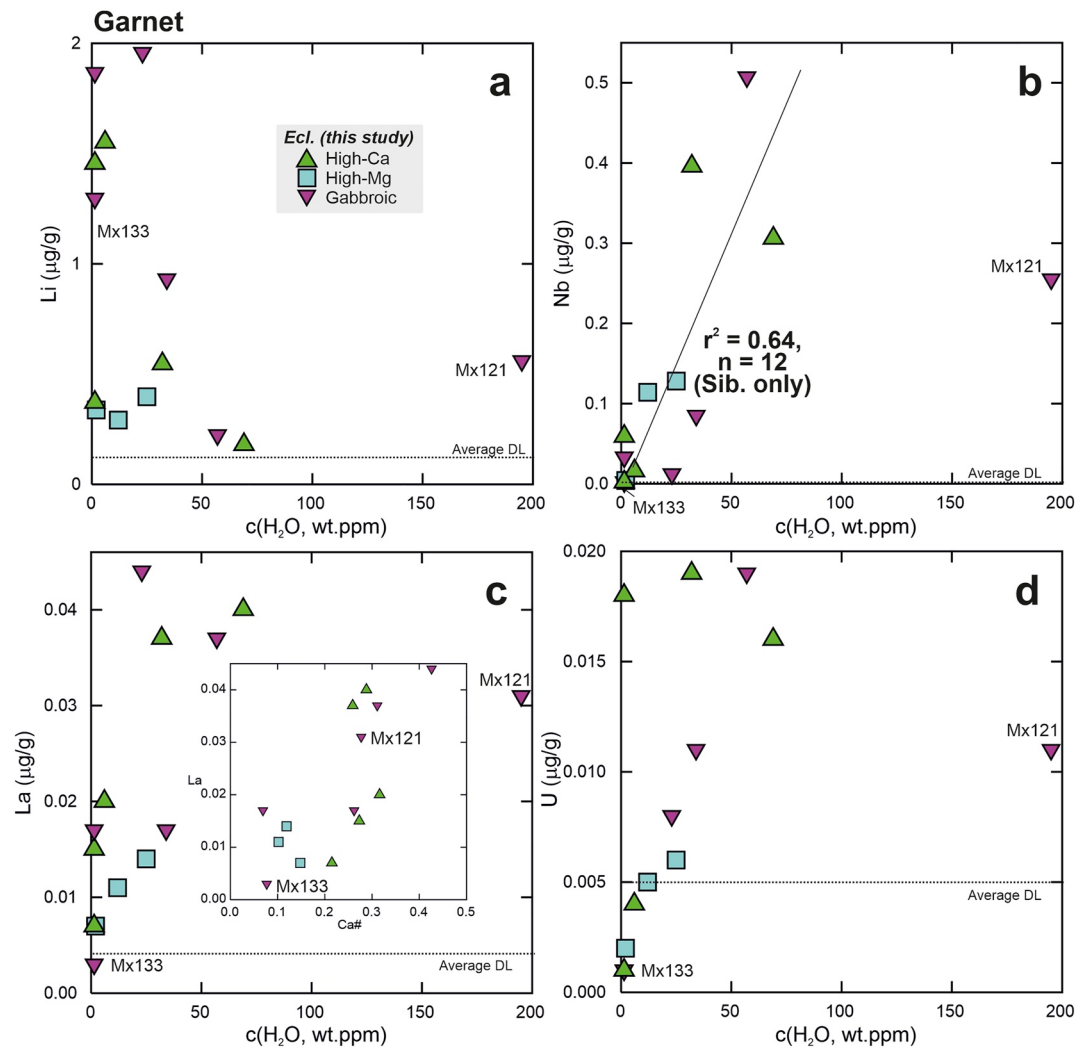


Figure 9. H₂O abundances (estimated uncertainty 20%) in garnet in eclogite xenoliths from the Siberian and Slave cratons (this study). High garnet c(H₂O) is weakly associated with (a) low Li ($r^2 = 0.19$), (b) high Nb ($r^2 = 0.64$), (c) La ($r^2 = 0.53$), and (d) U abundances ($r^2 = 0.45$; correlation coefficients for 11 samples from the Siberian craton); H₂O abundances in only two samples from the Slave craton (MX121, MX133—indicated separately) were quantified, which are consistent with the trends for garnet in eclogite xenoliths from the Siberian craton. The average detection limits for Li, Nb, La, and U in garnet were 0.14, 0.005, 0.004, and 0.005 µg/g, respectively (Aulbach et al., 2022).

Like Ca#, high temperatures facilitate the incorporation of some incompatible elements into garnet at the expense of clinopyroxene (e.g., O'Reilly & Griffin, 1995), which may help explain why high garnet c(H₂O) is associated with high Nb, LREE and U abundances (Figures 9b–9d). Clinopyroxene shows no correlation between H₂O abundances and Fe³⁺/ΣFe (Figure 10c), whereas garnet in samples from Udachnaya with the lowest H₂O contents also has low Mössbauer-derived Fe³⁺/ΣFe, while garnet in sample MX121 from Diavik has high c(H₂O) at its measured Fe³⁺/ΣFe (Figure 10d). The uptake of H₂O in clinopyroxene is favored by low fO_2 under experimental conditions (H. Liu & Yang, 2020), but no such relationship is evident for samples in this study (Figure 10e), possibly reflecting the narrower fO_2 range in eclogite xenoliths (<5 orders of magnitude) than in experiments (>8 orders of magnitude), and the superposition of compositional and temperature effects. However, there is a weak correlation of garnet c(H₂O) with fO_2 , as the two samples with the highest garnet c(H₂O) also yield the highest fO_2 estimates (>FMQ-3) (Figure 10f). More data are needed to ascertain whether this reflects an effect of fO_2 on garnet H₂O uptake that is opposite to that determined for clinopyroxene in the experiments of H. Liu and Yang (2020).

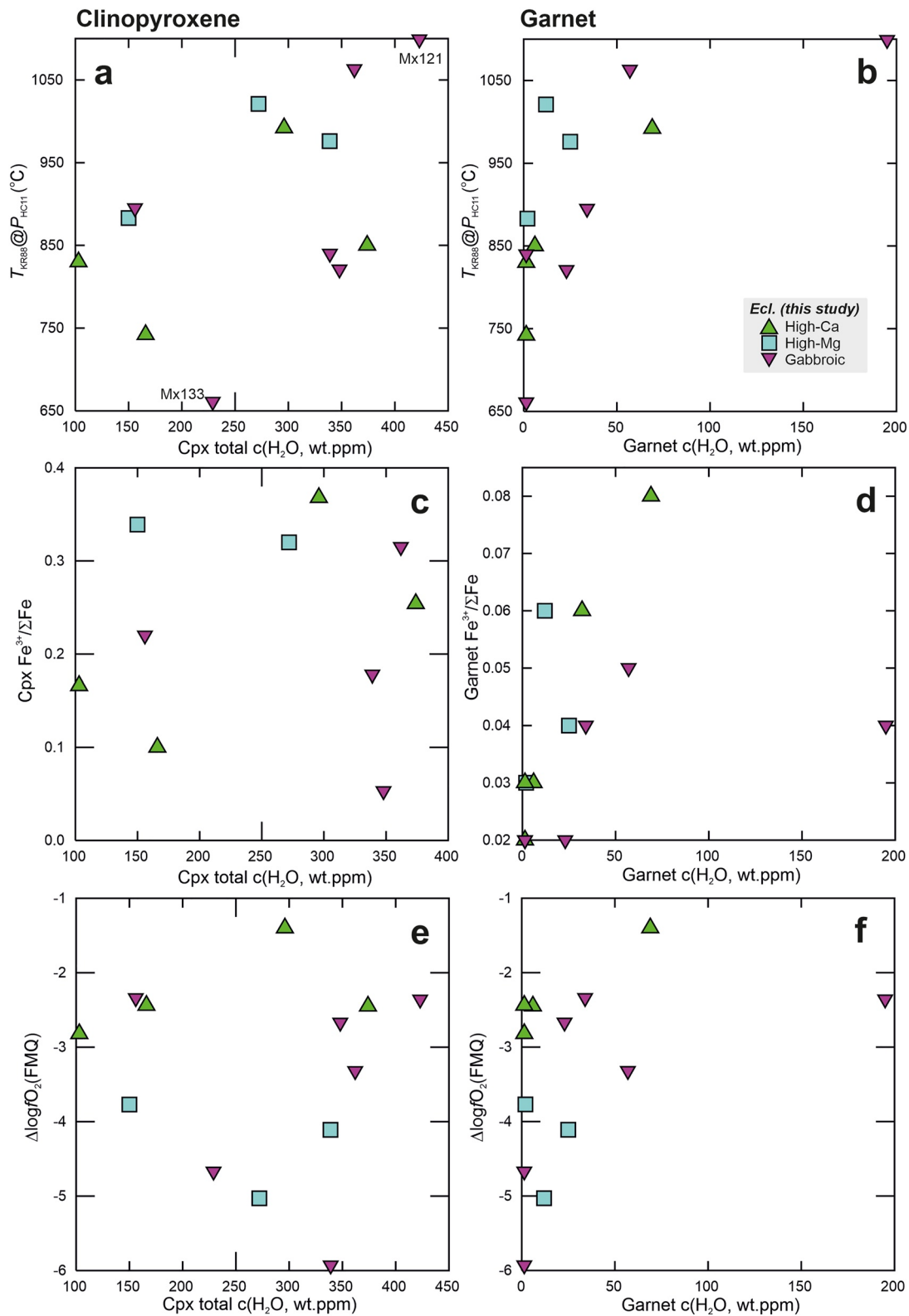


Figure 10. Bulk clinopyroxene (left) and garnet (right) H₂O abundances (estimated uncertainty 20%) in eclogite xenoliths from the Siberian and Slave cratons (data sources: this study, Taylor et al., 2016; Kolesnichenko et al., 2018; Radu et al., 2022). H₂O abundances in clinopyroxene and garnet as a function of (a, b) iteratively calculated temperature (see text and Figure S5 in Supporting Information S1), (c, d) mineral Fe³⁺/ΣFe, and (e, f) fO₂ relative to the fayalite-magnetite-quartz buffer.

6.3. H₂O Partitioning in Eclogite Minerals and Correlation With Fe³⁺/ΣFe

Water contents in eclogitic garnet are typically low and often reported as below detection in eclogite xenoliths from the Siberian craton (e.g., Agasheva et al., 2021; Kolesnichenko et al., 2018). In this study, both clinopyroxene and garnet H₂O abundances are fully quantified, allowing us to investigate the partitioning (or distribution *D*) of water between clinopyroxene and garnet as a function of various parameters. Although physicochemical effects on H₂O incorporation in either clinopyroxene or garnet are not strongly expressed in the eclogite xenoliths in this study, we note *D*(H₂O) regularities. Thus, the lowest *D* values (though not garnet c(H₂O)) are observed for samples with the highest garnet grossular content (Figure 11a) and for those with the highest ratio of diopside to jadeite component in clinopyroxene (Figure 11b). The lowest *D*(H₂O) values occur in samples with the highest equilibration temperatures (Figure 11c) and, less clearly, oxygen fugacities (not shown), making it difficult to

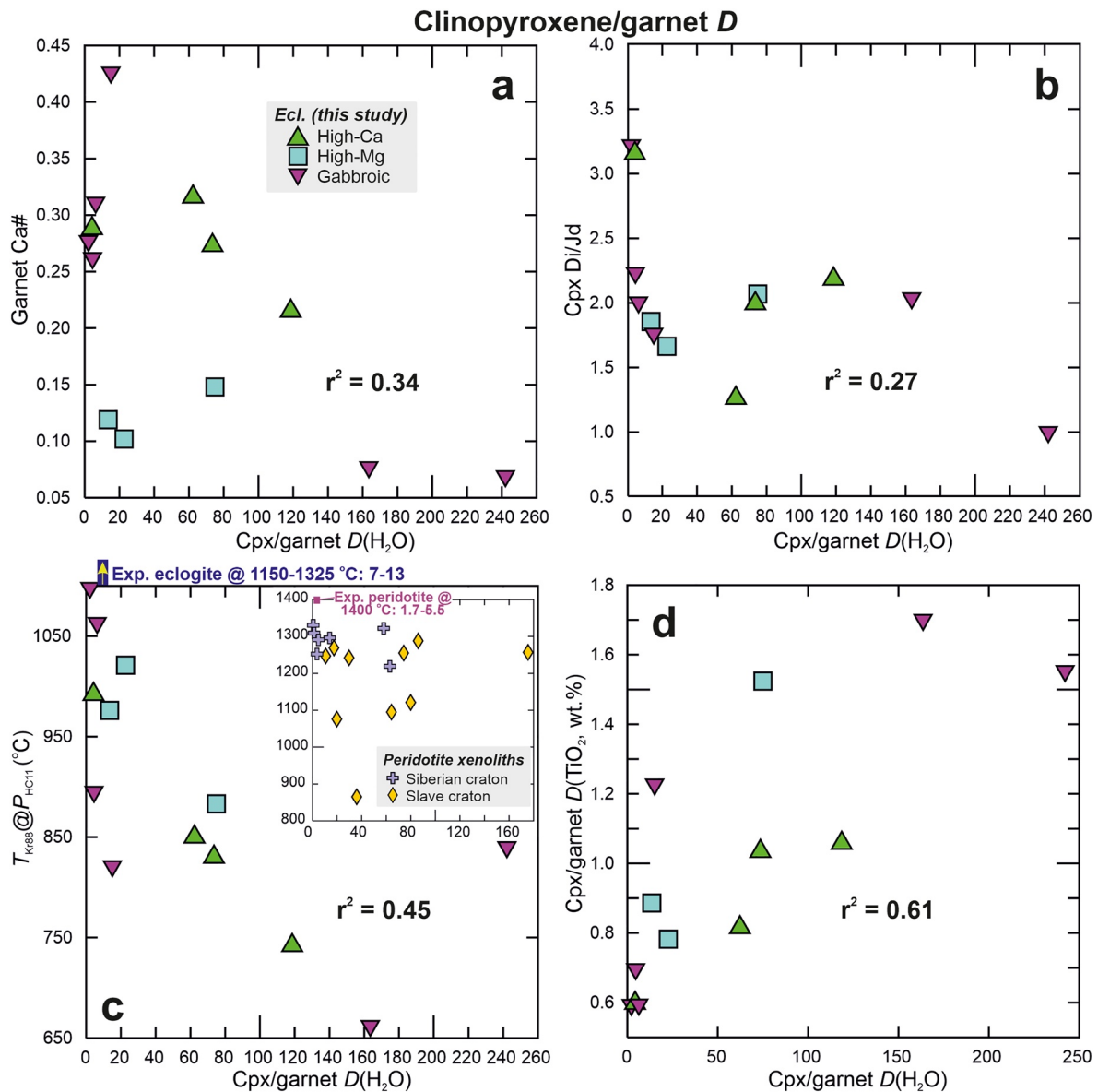


Figure 11. Partitioning *D* of H₂O (on a wt.ppm basis) between clinopyroxene and garnet in eclogite xenoliths from the Siberian and Slave cratons. The lowest *D* values are observed for samples with the highest (a) garnet Ca# (= grossular content), (b) ratio of diopside to jadeite component in clinopyroxene, (c) temperatures, and (d) the lowest *D*(TiO₂ on a wt.% basis). Shown for comparison as an inset in panel (c) are *D* values for peridotite xenoliths from the Siberian and Slave cratons (Doucet et al., 2014; Kilgore et al., 2020); also indicated are *D* values for experimental eclogitic clinopyroxene-garnet pairs in equilibrium with hydrous andesite melt (Aubaud et al., 2008) at temperatures in excess of those in eclogite xenoliths in this study, and, in the inset, *D* values for experiments in the peridotite system at 1400°C (Novella et al., 2014). Note that, along cold conductive geotherms characterizing the cratonic lithospheric mantle, pressure and depth increase along with temperature.

disentangle crystal-chemical and physical effects. $D(\text{H}_2\text{O})$ in the natural eclogite xenoliths in this study range to higher values, that is, 2.2–240 (Table 1), compared to values of 7–14 for clinopyroxene-garnet pairs in experiments at 3 GPa and 1150–1325°C in equilibrium with hydrous andesitic melt (Aubaud et al., 2008). This may be directly related to their lower temperatures of residence in the lithosphere prior to entrainment (<700–1100°C; Figure 11c). Clinopyroxene-garnet pairs in peridotite xenoliths from Udachnaya give $D(\text{H}_2\text{O})$ of 0.6–63 (Doucet et al., 2014; Ragozin et al., 2014), while pairs in the study of Kilgore et al. (2020) yield $D(\text{H}_2\text{O})$, from 11 to 180. In both studies $D(\text{H}_2\text{O})$ is unrelated to temperature, thus revealing significantly different relations of H_2O partitioning in eclogitic versus peridotitic clinopyroxene-garnet pairs.

As outlined above, the incorporation of incompatible trace elements in garnet coexisting with clinopyroxene is favored by high grossular content and temperature, and this seems to similarly hold for H_2O , underlining similarities in the behavior of water and incompatible elements. Indeed, H_2O is considered to have partitioning behavior similar to those of LREE or MREE (Aubaud et al., 2004; Denis et al., 2015). In this light, rather than pointing to a primary control on H_2O partitioning, the anticorrelation of $D(\text{H}_2\text{O})$ values with $\text{Fe}^{3+}/\Sigma\text{Fe}$ may simply reflect the fact that Fe^{3+} is incompatible (e.g., O'Neill et al., 2018). The distribution of Fe^{3+} between eclogite clinopyroxene and garnet appears to be affected by crystal chemistry, temperature and $f\text{O}_2$, whereas the uptake of Fe^{3+} in either clinopyroxene or garnet is much less clearly related to these parameters (Aulbach et al., 2019, 2022), similar to observations for H_2O in this study. As the inter-mineral distribution of TiO_2 is also temperature-dependent (Aulbach, 2020), samples in this study show coherent correlations of $D(\text{H}_2\text{O})$ with $D(\text{TiO}_2)$ ($r^2 = 0.61$, $n = 12$; Figure 11d), as is true for $D(\text{Fe}^{3+}/\Sigma\text{Fe})$ (Aulbach et al., 2022). Therefore, if H_2O abundance of one mineral only is known, $c(\text{H}_2\text{O})$ of the other mineral, and therefore bulk $c(\text{H}_2\text{O})$, may be roughly estimated using the distribution of TiO_2 , which is easily determined in both minerals, as a proxy.

6.4. Eclogite Contribution to Seismic Velocity and Density Signals in the Siberian Craton

Estimates of the abundance of cratonic eclogite in the lithosphere vary widely. They range from a few volume percent based on petrologic and heat flow constraints (e.g., McLean et al., 2007; Russell et al., 2001; Schulze, 1989) to ~20% based on joint density and gravity constraints and the observation that cratonic shear-wave velocities are higher than those that can be generated by peridotite alone (Garber et al., 2018). The upper mantle structure beneath the Siberian craton is not well constrained due to a dearth of seismic stations and events (Cherepanova & Artemieva, 2015), but anomalous V_p of up to 8.9 km/s has been determined (Melnik et al., 2015). In contrast, laboratory measurements on peridotite and eclogite xenoliths have yielded maximum V_p of 8.6 km/s, which could be higher assuming high modes and, in peridotite, favorable orientation of olivine (Bascou et al., 2011; Kobussen et al., 2006). Melnik et al. (2015) found three velocity layers, suspecting that eclogite contributes to the middle one with the highest V_p . The V_p estimate for eclogite xenoliths in this study is relatively high at 8.4–8.8 km/s (Table 1), but given the estimated eclogite volume in the regional lithospheric mantle (4% based on its abundance in the xenolith suite from Udachnaya; Sobolev, 1990), the bulk of the velocity signal likely comes from the dominantly peridotitic mantle.

Based on gravity data, Artemieva et al. (2019) suggest that the lithospheric mantle beneath the Siberian craton is compositionally layered, with a density increase at 160–180 km. Lithospheric layering is indicated by chemical composition of xenoliths (Doucet et al., 2013; Z. Liu et al., 2022) and xenocrysts (Ashchepkov et al., 2017; Griffin et al., 1999), but with different conclusions regarding its magnitude and the distribution of lithologies with depth. A recent detailed study of ~170 garnet peridotites finds harzburgites dominantly above 190 km, with little variation except for an anomalously hot, clinopyroxene- and garnet-rich, phlogopite-bearing layer at ~135 km, as well as a hot and Fe-enriched lithospheric base below 190 km (Z. Liu et al., 2022). This might cause some density layering, although the extent to which Fe enrichment is offset by increasing temperature requires assessment. The eclogite xenoliths under investigation cover a range of ~115–180 km, but are not concentrated at any depth (Figure 12a); this is true for eclogite xenoliths from the Siberian craton and their bulk FeO contents generally ($n = 126$; Figure 12b) that show no density correlation with depth. Therefore, eclogite does not cause any density layering. The overall in situ density of the lithosphere beneath the Siberian craton is ~3.24–3.28 g/cm³ (Artemieva et al., 2019) compared to 3.53–3.71 g/cm³ for eclogite xenoliths in this study. With its density significantly greater than for peridotite (Garber et al., 2018), eclogite contributes markedly to the overall gravity signal, qualitatively placing upper limits on its share in the cratonic mantle or lower limits on the fraction of depleted and less dense harzburgite that must be present, which remains unquantified, however.

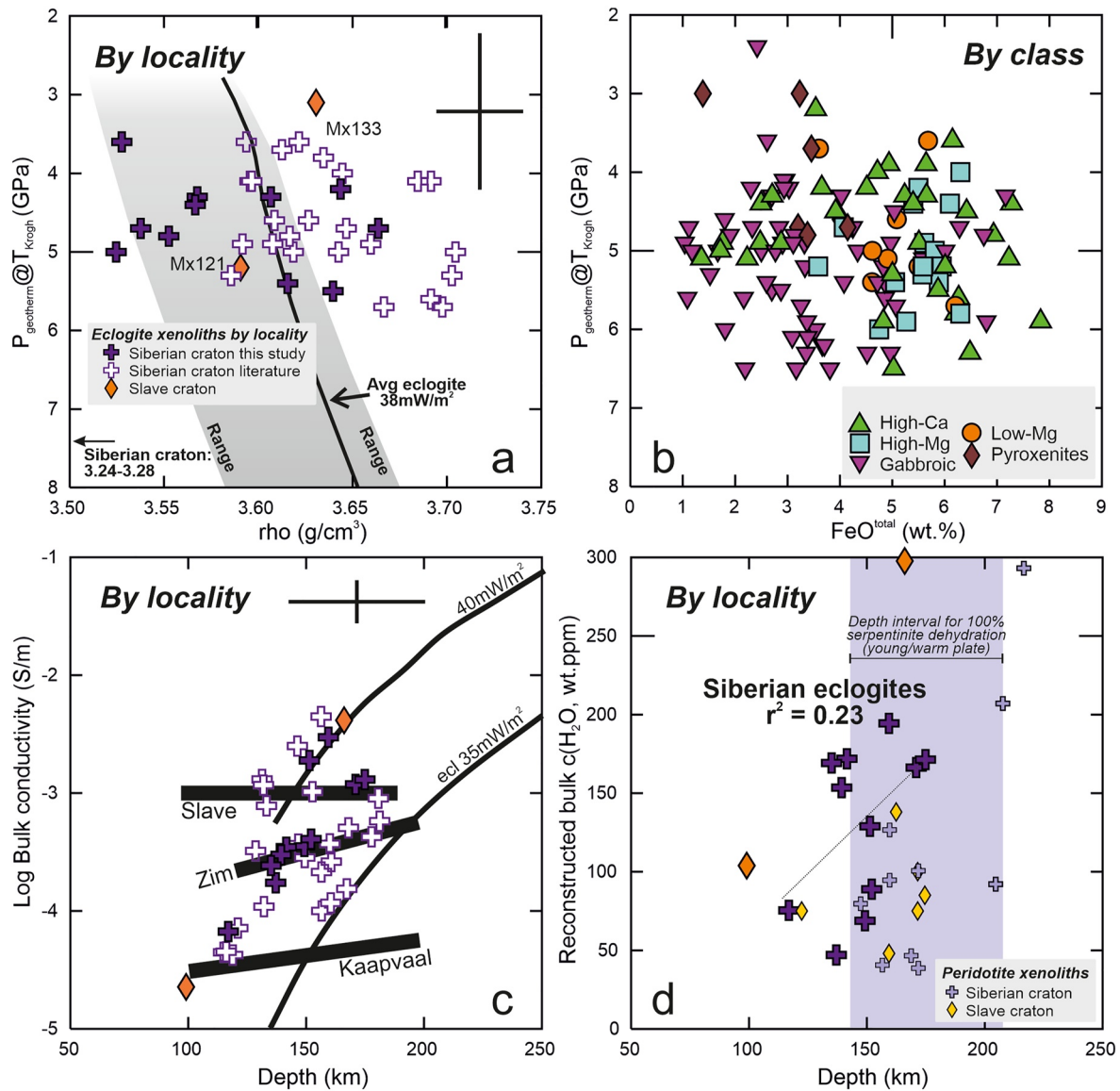


Figure 12. Physical properties of eclogite and pyroxenite xenoliths from the Siberian and Slave cratons (data sources: this study—Table 1, Taylor et al., 2016; Kolesnichenko et al., 2018; Radu et al., 2022). (a) Density for samples by locality and (b) FeO content for eclogite and pyroxenite xenoliths (by eclogite class) from the database in Stachel et al. (2022) illustrate the lack of compositional layering; note lower average FeO content for gabbroic eclogites which have plagioclase-rich cumulate protoliths. Shown for comparison in panel (a) are results for average eclogite (solid black line) as well as low-Mg and high-Mg extremes (gray field) from Garber et al. (2018) for a geothermal gradient 38 mW/m^2 . The uncertainty in pressure is assumed to be 1 GPa, and the density uncertainty reflects a total 10% uncertainty in the mineral modes assumed for bulk rock reconstruction (from Aulbach et al. (2020)). The range of in situ densities for the Siberian cratonic lithosphere (Artemieva et al., 2019) is indicated on the bottom left of panel (a). (c) Electrical conductivity (for dry garnet and wet clinopyroxene; Dai & Karato, 2009; Zhao & Yoshino, 2016) and (d) reconstructed bulk H_2O abundance (i.e., $c(\text{H}_2\text{O})$ weighted by modes of 0.55 garnet and 0.45 clinopyroxene), both of which weakly increase with depth; the estimated uncertainty for bulk $c(\text{H}_2\text{O})$ is estimated at 30%, arising from 20% uncertainty on mineral H_2O abundances and 10% uncertainty on mineral modes used in the reconstruction. Shown for comparison in panel (c) are calculated electrical conductivities for an average eclogite composition along conductive geotherms of 35 (lower electrical conductivity) and 40 mW/m^2 (higher electrical conductivity) (thin solid black curves) as well as electrical conductivities derived from magnetotelluric studies in various cratons (Zim—Zimbabwe) from Garber et al. (2018) (thick black bars). The depth uncertainty is derived from pressure uncertainty in panel (a), average electrical conductivity uncertainty arising for a pressure uncertainty 1 GPa and a temperature uncertainty of 60°C is $10^{0.38} \text{ S/m}$. Shown for comparison in panel (d) are bulk H_2O abundances reported for peridotite xenoliths from the Siberian (Doucet et al., 2014; Ragozin et al., 2014; Kolesnichenko et al., 2017) and Slave (Kilgore et al., 2020) cratons, as well as the depth interval over which serpentinite in a young (40 Ma) and warm oceanic plate dehydrates according to modeling in Rüpke et al. (2004).

6.5. Water in Xenolithic Eclogite Versus Peridotite, Electrical Conductivity, and Longevity of Cratonic Lithospheric Mantle

Cratonic mantle is typically electrically resistive, plausibly relating to its strong depletion and attendant H₂O extraction (e.g., Peslier et al., 2010), although intra-lithospheric increased conductivity is occasionally observed (Bettac et al., 2023; Jones et al., 2001; Le Pape et al., 2021). High proportions of H₂O-rich eclogite or pyroxenites have been invoked to explain conductivity anomalies in the crust and upper mantle (Dai et al., 2016; H. Liu et al., 2019; Yang & McCammon, 2012). Electrical conductivity in NAMs is strongly temperature-dependent but also increases with increasing mineral H₂O content, depending on where protons are sited (e.g., Jones et al., 2009; H. Liu et al., 2019; Schlechter et al., 2012; Zhao & Yoshino, 2016). For example, in the garnet, the effect of H₂O on electrical conductivity diminishes with increasing temperature and increases with pressure (Dai & Karato, 2009), such that along conductive geotherms common in the lithospheric mantle, the effects of pressure and temperature should to some extent cancel each other out. In this study, neither electrical conductivity (Figure 12c) nor calculated bulk H₂O content clearly correlate with depth (Figure 12d). The calculated electrical conductivities (using the relationship for wet clinopyroxene in Zhao and Yoshino (2016), and dry garnet in Dai and Karato (2009)) for two eclogite xenoliths from the central Slave craton vary widely (10^{-4.7}–10^{-2.4} S/m), and bracket bulk conductivities for the Slave lithosphere reported in Garber et al. (2018) (Figure 12c). There are no constraints on mantle conductivity in the Siberian craton that we are aware of. The electrical conductivities estimated here for eclogite xenoliths (10^{-4.4}–10^{-2.4} S/m; Table 1) lie mostly between those of the more resistive Kaapvaal cratonic mantle and the relatively conductive Slave cratonic mantle, with some higher values. This suggests that bulk conductivity is a blunt tool to place upper or lower limits on eclogite abundance in the lithospheric mantle. However, as this study focuses on pristine eclogite xenoliths, the true extent of possible metasomatic hydration in this rock type has yet to be determined.

The weak correlation of bulk rock H₂O content in Siberian eclogites with depth (Figure 12d) suggests that the cratonic mid-lithosphere is drier than the deep lithosphere. At Udachnaya, greater H₂O abundances are also inferred for deeper than for shallower peridotite xenoliths (Doucet et al., 2014). In contrast, peridotite xenoliths from shallow depths in the central Slave craton contain more H₂O (Kilgore et al., 2020). Taking H₂O content as a proxy for viscosity may imply that at Udachnaya, the deep lithosphere may have been close to destabilization (at the time of kimberlite eruption) because craton longevity is controlled by the viscosity contrast between lithosphere and ambient convecting mantle (e.g., Paul & Ghosh, 2020; H. L. Wang et al., 2014). Similarly, Peslier et al. (2017) calculated viscosities for the deep Siberian peridotite lithosphere that are similar to those of the ambient asthenospheric mantle.

6.6. Long-Term Retention of H₂O in the Eclogite Xenolith Source

Many studies have found garnet and clinopyroxene to be robust to diffusional H exchange with kimberlite during entrainment (Demouchy et al., 2006; Peslier, 2010; Peslier & Luhr, 2006; Sundvall & Stalder, 2011). This is consistent with the observation that Fe³⁺/ΣFe in clinopyroxene and garnet in this study are unrelated to H₂O (Figures 10c and 10d), as dehydrogenation during ascent may be compensated by concomitant iron oxidation (e.g., Ingrin & Skogby, 2000). This implies that Fe³⁺/ΣFe in eclogite xenoliths reflects pre-entrainment conditions that can inform us on processes related to their petrogenesis (e.g., Aulbach et al., 2022).

Enrichment in H₂O due to mantle metasomatism by a kimberlite-like agent prior to xenolith entrainment has been implicated in some studies (e.g., Doucet et al., 2014; Huang et al., 2014; Kolesnichenko et al., 2017; Peslier et al., 2012). The samples in this study do not contain obvious metasomatic minerals (e.g., phlogopite) and are LREE-depleted, with relatively flat MREE and HREE patterns (Figure 1c), except for sample UV65-15, which features a peculiar depletion in MREE-HREE that is also observed in other eclogite xenoliths from Udachnaya (Mikhailenko et al., 2021) and Obnazhennaya (Radu et al., 2022). Given that LREE or MREE have partitioning behavior similar to that of H₂O (Aubaud et al., 2004; Denis et al., 2015), H₂O enrichment during mantle metasomatism is not considered to have occurred in the samples in this study. This is corroborated by a comparison of bulk-rock c(H₂O) using measured H₂O contents in clinopyroxene and garnet to hypothetical abundances if these minerals interacted with a typical mantle metasomatic melt. The latter is here taken as a kimberlite containing 3 wt.% H₂O (as argued by Aulbach et al., 2020), and hypothetical H₂O abundances are calculated using mineral-melt *D*(H₂O) as a function of Al₂O₃ in clinopyroxene and of TiO₂ in garnet according to Aubaud et al. (2008). Except for sample MX121, the reconstructed bulk H₂O concentrations fall well below those expected for samples in equilibrium with kimberlite (Figure 13a).

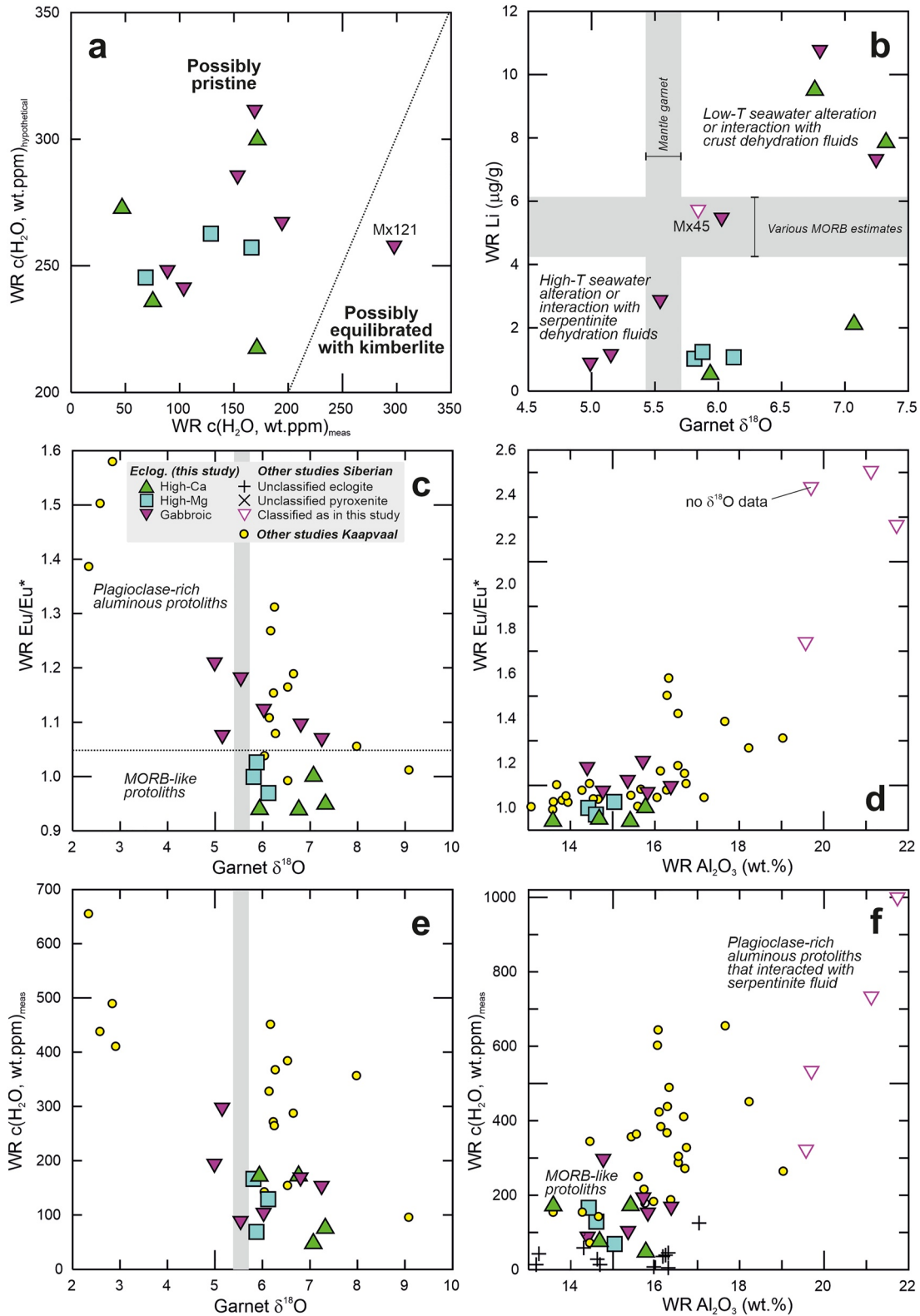


Figure 13.

Circumstantial evidence for long-term retention of ancient H₂O signatures is provided by the observation that somewhat higher c(H₂O) is observed at greater depth, that is, temperature along steady-state conductive geotherms, where diffusive equilibration with the dominant but H₂O-poorer peridotites (Figure 12d) would be expected to be most efficient, and that, at least in the Slave craton, contrasting trends of H₂O distribution are observed for peridotite and eclogite xenoliths. Similarly, extremely high H₂O contents in eclogite xenoliths from Obnazhennaya (Siberian craton) were taken to indicate the presence of at least a locally H₂O-rich eclogite reservoir in a much H₂O-poorer peridotitic mantle (Radu et al., 2022). This may be linked to the large grain size of mantle eclogite (mm to cm) and low effective diffusivities during fast kimberlite ascent, which together preclude homogenization at the grain scale during transport in the kimberlite and at the (sub-)km-scale at geological timescales (Demouchy, 2010; Demouchy & Bolfan-Casanova, 2016; Marshall et al., 2018). If so, the retention of signatures acquired during eclogite formation billions of years ago (ca. 2.7 Ga for eclogite xenoliths from the Siberian craton, 1.9 Ga for those from the Slave craton) until kimberlite magmatism in the Phanerozoic may provide constraints on the size of eclogite heterogeneities in the lithospheric mantle.

6.7. Effect of Seawater Alteration and Origin of High H₂O Contents in Deep Oceanic Crust

Given the retention of H₂O in eclogite xenoliths, their H₂O contents may relate to processes occurring during weathering or subduction of the ocean floor in the Archean (Udachnaya) and Paleoproterozoic (Diavik). Oxygen isotope compositions are typically used to assess the effect of seawater alteration in eclogite xenoliths (Korolev et al., 2018), which produces sub-mantle δ¹⁸O at high temperatures (>~250°C) and supra-mantle δ¹⁸O at low temperatures (Gregory & Taylor, 1981; Muehlenbachs & Clayton, 1972a, 1972b). Garnet in Siberian eclogite xenoliths in this study has δ¹⁸O (+4.99 to +7.32) well within the previously reported range (Jacob et al., 1994; Shatsky et al., 2016; J. Sun et al., 2020). Samples with high δ¹⁸O have high reconstructed bulk rock Li abundances (Figure 13b). The two samples with the lowest garnet δ¹⁸O in the data set (+4.99 and +5.15), below that inferred for mantle garnet (+5.4 to +5.7, Ickert et al., 2013), may reflect the incipient high-temperature seawater alteration. Their sub-mantle garnet δ¹⁸O is accompanied by low bulk-rock Li abundances compared to fresh MORB (4.3–6.1 μg/g, Arevalo & McDonough, 2010; Gale et al., 2013; S.-S. Sun & McDonough, 1989), which agrees with findings that Li is added during low-temperature, but leached during high-temperature seawater alteration (Staudigel, 2005). When samples from the Kaapvaal craton are also considered, it appears that low garnet δ¹⁸O is accompanied by high Eu/Eu* (Figure 13c), pointing to a plagioclase-rich cumulate protolith, although it should be noted that globally there is no correspondence between the type of protolith and oxygen isotopic signature (Korolev et al., 2018). In turn, high Eu/Eu* is associated with high Al₂O₃ contents, which is particularly obvious when samples from Obnazhennaya (no δ¹⁸O data) and from the Kaapvaal craton, with even stronger cumulate character, are considered together with data from Udachnaya (Figure 13d). Of note, gabbroic eclogites with low δ¹⁸O and high Al₂O₃ are clearly associated with high H₂O abundances (Figures 13e and 13f). Similarly, Agasheva et al. (2021) report c(H₂O) of 35–225 wt.ppm for eclogite xenoliths with gabbroic protoliths from the Grib kimberlite (Kola craton), compared to 20–36 wt.ppm for those with basaltic protoliths.

Eclogites in the mantle reside at temperatures above the wet eclogite melting reaction (Figure S5 in Supporting Information S1), where Li becomes incompatible (Kessel et al., 2005). Moreover, the slab top would experience earlier dehydration than deeper parts of the oceanic crust (van Keken et al., 2011). As a consequence, the high bulk Li abundances and heavy O in samples with upper crustal protoliths may have been acquired after melt loss by interaction with fluids resulting from the dehydration of deeper portions of altered oceanic crust. As the δ¹⁸O of some oceanic serpentinite ranges to very low, sub-mantle values (+0.8 to +6.7, average δ¹⁸O +3.3, Barnes

Figure 13. Reconstructed bulk eclogite H₂O abundances (estimated uncertainty 30%, see caption to Figure 12) and various compositional indicators of seawater alteration and igneous oceanic protoliths. (a) Bulk H₂O abundances reconstructed from measured H₂O abundances (“meas.”) in clinopyroxene and garnet versus those calculated for these minerals in equilibrium with a kimberlite containing 3 wt.% H₂O (“hypothetical”; for rationale see Aulbach et al. (2020)) based on equations in Aubaud et al. (2008). This illustrates that most samples would not have been in equilibrium with a kimberlite-like metasomatic agent, the signatures of which are typically detected in metasomatized eclogite and pyroxenite xenoliths. (b) Oxygen isotopic composition (notated as δ¹⁸O, with an estimated uncertainty of 0.3) in garnet as a proxy for low- and high-temperature seawater alteration versus abundances of Li, a fluid-mobile element, in reconstructed whole rocks (results for MX45 with overestimated H₂O abundances are also displayed); shown for comparison is the range of Li abundances in various estimates of average NMORB composition (Arevalo & McDonough, 2010; Gale et al., 2013; S.-S. Sun & McDonough, 1989) and range of mantle δ¹⁸O (Ickert et al., 2013). (c) δ¹⁸O in garnet versus Eu/Eu* as a proxy for cumulate versus MORB-like melt oceanic crustal protoliths in reconstructed whole rocks; samples from the Kaapvaal craton are shown for comparison (yellow circles). (d) Very high Al₂O₃ contents are reported in four samples with the highest Eu/Eu* from Obnazhennaya (no δ¹⁸O data), therefore greatest normative plagioclase content. (e) Garnet δ¹⁸O and (f) bulk Al₂O₃ contents versus reconstructed bulk eclogite c(H₂O) (Data sources: this study; Smyth et al., 1991; Snyder et al., 1995; Matsyuk et al., 1998; Koch-Müller et al., 2004; Huang et al., 2014; Taylor et al., 2016; Kolesnichenko et al., 2018; Radu et al., 2022).

et al., 2006; Wenner & Taylor, 1973), low $\delta^{18}\text{O}$ at low Li abundances in gabbroic eclogites may be imparted when serpentinite-derived fluids interact with the proximal deep oceanic crust (although others have suggested heavier $\delta^{18}\text{O}$ of 8‰–10‰ for serpentinite-derived fluid, Alt et al., 2012). In this interpretation, variations in $\delta^{18}\text{O}$ need not be generated exclusively on the ocean floor, but would in any case require fluids tapping a seawater-altered reservoir. Importantly, high $c(\text{H}_2\text{O})$ is linked to high Al_2O_3 in bulk rocks (Figure 13f) via their enrichment in aluminous, jadeite-rich clinopyroxene (Figure 14a). As the stabilization of jadeite and omphacite requires high-pressure metamorphism (Holland, 1980; Kushiro, 1969), combined with all other observations, we propose that it is the high Al_2O_3 content of clinopyroxene in metamorphosed deep oceanic crustal cumulates with high normative plagioclase, rather than hydration on the ocean floor, that causes their enrichment in H_2O , as illustrated in Figure 14.

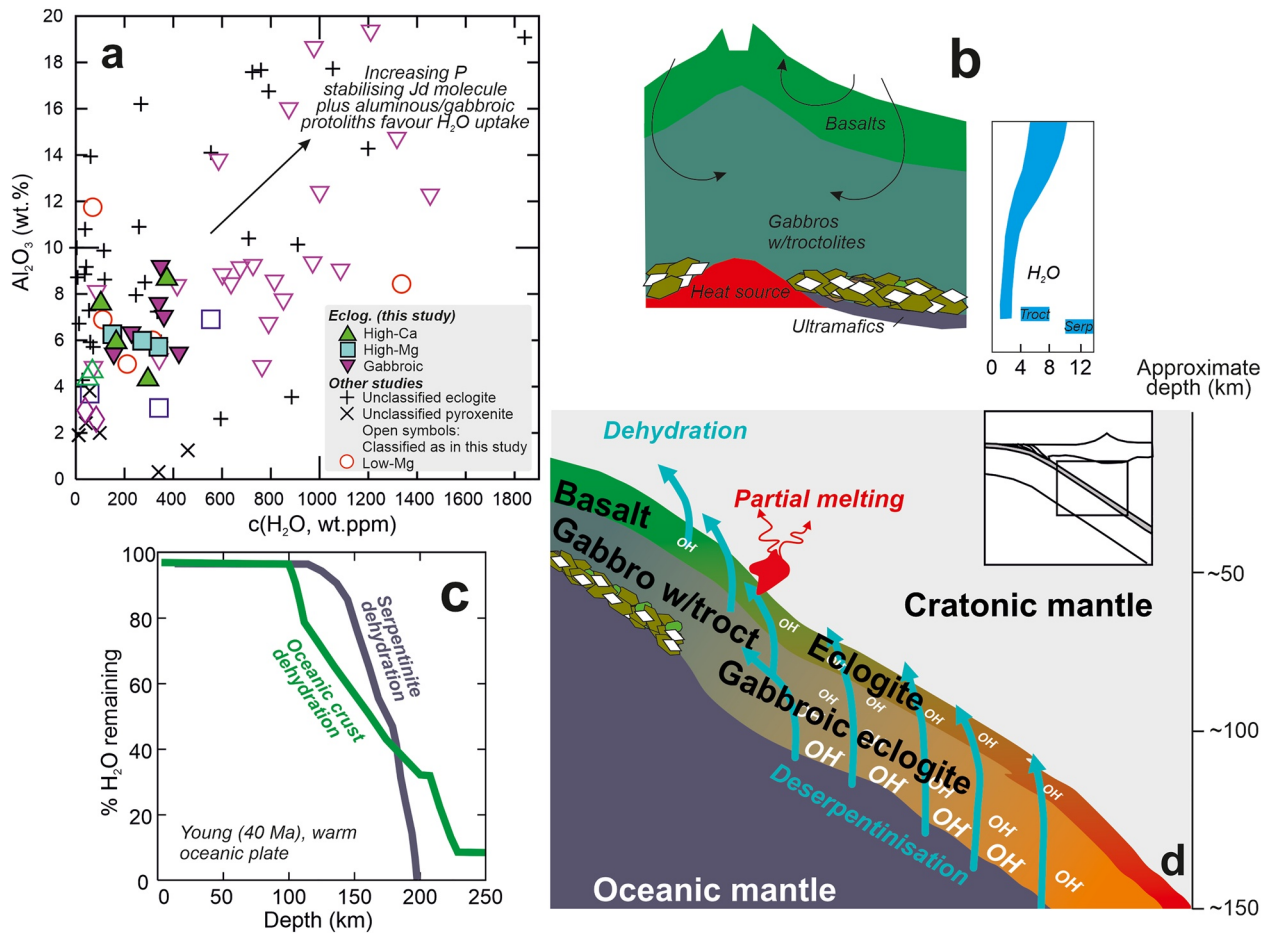


Figure 14. Models for hydration, dehydration, and rehydration of oceanic slabs and H_2O capture predominantly in deep oceanic crust. (a) Al_2O_3 content in clinopyroxene (wt.%, by eclogite class—note that only samples for which both major and trace elements in both garnet and clinopyroxene are reported can be classified), as a measure of the normative plagioclase mode in the igneous oceanic cumulate protolith and the pressure-dependent stabilization of the jadeite molecule, versus $c(\text{H}_2\text{O})$ in clinopyroxene (data from other studies as in Figure 1 plus data from the Kaapvaal craton in Smyth et al. (1991) and Huang et al. (2014)). (b) Model mid-ocean ridge section with various average H_2O contents for the upper and lower oceanic crust, and typical contents in troctolites (troct.) and strongly serpentinized oceanic mantle (after Schmidt and Poli (2014)). (c) Relative water release (in %) from various components of an oceanic slab as a function of slab depth for a young (therefore warm) oceanic plate (from Rüpke et al. (2004)) as an approximation to an Archean dehydration profile and illustrating massive H_2O flushing from serpentinized mantle in the depth interval from which eclogite xenoliths were entrained (cf. Figure 12d). (d) Cartoon illustrates how serpentinite-derived fluids liberated at depth where basalt and gabbros plus troctolites are metamorphosed to eclogite and gabbroic eclogite, respectively, would more strongly hydrate the proximal, metamorphosed Al_2O_3 -rich parts of the oceanic crust than the, on average, Al_2O_3 -poorer upper oceanic crust (depths are approximate: the basalt- or gabbro-to-eclogite transition may vary according to bulk composition, and the dehydration of various slab lithologies according to the exact subduction geotherm).

6.8. Insights From Pristine Mantle Eclogite Xenoliths on Deep Water Transport Through Time

As outlined above, xenolithic eclogite originated as spreading ridge-derived oceanic crust in the Paleoproterozoic to Archean (Aulbach & Jacob, 2016; Aulbach & Smart, 2023; Jacob, 2004). Although NAMs in orogenic eclogites may have high $c(\text{H}_2\text{O})$ (e.g., Katayama et al., 2006), they are unlikely to be representative of those in deeply subducted and metamorphosed oceanic crust. First, it is increasingly recognized that exhumed metamorphic rocks are not representative of the total subducted lithosphere (e.g., Penniston-Dorland et al., 2015; Y. Wang et al., 2023). Second, the exhumation of orogenic eclogites is slow (mm/yr for oceanic settings) and accompanied by fluid-fluxing allowing exhumation (Agard et al., 2009). In contrast, chemically and mineralogically diverse eclogite xenoliths are exhumed from diamond-stable conditions in hours or days in fast-erupting kimberlites (e.g., Peslier et al., 2008). The pristine eclogite xenoliths studied here thus allow insights into the minimum amount of hydrogen that could have been transported into the convecting mantle in Archean and Paleoproterozoic subduction zones, bearing in mind that in addition to hydroxyl, molecular hydrogen (H_2) may be present in eclogitic NAMs (Moine et al., 2020).

The effects of Archean seafloor weathering may to some extent have been similar to those today (e.g., Kusky et al., 2001), which is plausible from a stable isotope perspective, in particular $\delta^{18}\text{O}$ and triple O isotope compositions requiring low-temperature seawater alteration (e.g., Korolev et al., 2018; McGunnigle et al., 2022). Pressure-temperature conditions estimated for eclogite xenoliths and probable Archean subduction paths indicate that they would have been completely dehydrated and crossed the wet eclogite solidus (Figure S5 in Supporting Information S1), consistent with the fact that eclogite xenoliths contain no hydrous minerals, except those affected by later hydrous mantle metasomatism, which produces secondary phlogopite (Jacob et al., 2009) or amphibole (Smart et al., 2021). However, not all eclogite xenolith sources need to have had sufficient initial H_2O contents to stabilize hydrous minerals or undergo partial melting. Regardless, most crustal H_2O is estimated to be lost from modern slabs at subarc depths at the latest (Figure 14c), probably earlier in warmer Precambrian subduction zones, leaving NAMs in eclogite as the main carriers of oceanic crust-derived H_2O into the deep mantle.

Of the oceanic crust, 70% is plutonic, the remainder being upper extrusive oceanic crust and sheeted dike complexes (White & Klein, 2014). The proportion of eclogite xenoliths with cumulate (50%–60%) and MORB-like protoliths in the global database is similar (Stachel et al., 2022), bearing in mind that mantle metasomatism mutes crustal signatures including Eu anomalies (Aulbach et al., 2020). Excluding literature eclogite xenoliths with chondrite-normalized $\text{Ce}/\text{Yb} > 1$ as a measure of metasomatic enrichment (three of four eclogite xenoliths Obnazhennaya with extremely LREE-depleted compositions below detection are considered pristine), and taking Eu/Eu^* of 1.05 as a cut-off to distinguish the cumulate and melt-like protoliths (Aulbach & Jacob, 2016), 19 gabbroic eclogites have a median reconstructed bulk Al_2O_3 content of 16.4 versus 14.7 wt.% for 15 MORB-like eclogites, which is similar to average modern lower oceanic crust at 16.7 wt.% (Coogan, 2014) and MORB at 14.8 wt.% (White & Klein, 2014). Gabbroic eclogites have median reconstructed bulk $c(\text{H}_2\text{O})$ of 290 wt.ppm (average 240 ± 120 wt.ppm 1σ), whereas MORB-like eclogites have median bulk $c(\text{H}_2\text{O})$ of 140 wt.ppm (average 160 ± 140 wt.ppm). To remove the weight of those outliers, median values are here used to estimate the bulk H_2O abundance in ancient oceanic crust. Based on pristine eclogite xenoliths, which derive from depths >100 km, bulk paleo-oceanic crust had an estimated $c(\text{H}_2\text{O})$ of 240 wt.ppm H_2O , obtained by weighting the rock distribution in modern oceanic crust (70% gabbroic eclogites at median 290 wt.ppm vs. 30% MORB-like eclogites at 140 wt.ppm).

Magni et al. (2014) estimated that H_2O could have been subducted to the mantle in the Archean but with significantly reduced efficiency (down by 70%) based solely on warmer mantle potential temperature T_p , although this may be reduced to nil when plate velocities or ages are also varied. H. Liu et al. (2021) model H_2O abundances in eclogitic omphacite and garnet based on the resistive nature of modern subducted oceanic crust at 70–120 km, and suggest that these minerals contain <400 and <80 wt.ppm H_2O , respectively, corresponding to a bulk eclogite with ~ 220 wt.ppm H_2O (assuming mineral proportions as in this study), similar to our estimate. Thus, H_2O recycling efficiency in the Archean may have been not much different from that today. Given that plate velocities were higher in a warmer Archean mantle, which aids H_2O retention (Magni et al., 2014), but is in part offset by lower average plate age (van Hunen & van den Berg, 2008), this may indicate an upper limit on the difference between Archean and modern T_p , that is, a warm rather than hot Archean convecting mantle (Aulbach & Arndt, 2019; for a different view see Herzberg et al. (2010)). Water outgassing via magmatism is also more efficient for higher mantle T_p (Dong et al., 2021), and must be compensated in order to maintain

surface oceans but also some fraction of emerged continental landmasses on Earth's surface (e.g., Andrault & Bolfan-Casanova, 2022; Korenaga, 2011). Deep H₂O ingassing, in particular in deep oceanic crustal cumulates (Figure 14d) from the Archean onwards may help to satisfy this requirement. If, on the other hand, net hydration of the mantle has occurred over time (Korenaga et al., 2017), sources other than oceanic crust, such as hydrated oceanic mantle, may be needed.

7. Conclusions

In this study, new FTIR-derived H₂O concentration data in clinopyroxene and garnet from Archean and Paleoproterozoic eclogite xenoliths from Udachnaya (Siberian craton) and Diavik (Slave craton), respectively, as well as SIMS-derived garnet δ¹⁸O values were combined with literature data to determine the inter-mineral partitioning behavior of H₂O, gauge the effects of H₂O in this lithology on electrical conductivity, test to what extent H₂O content reflects pre-entrapment compositions, and assess the viability of deep H₂O subduction in ancient oceanic crust. The main findings are:

- The orientation of the OH dipole in clinopyroxene, captured as the ratio of γ -over α -polarized component, shows marked correlations with concentrations of several trace elements (Li, Ag, Nb), suggesting an association with specific lattice sites. The positive correlation of the γ/α ratio with clinopyroxene Fe³⁺/ΣFe and with temperature suggests that it may be a useful proxy for the iron valence state if the temperature effect is accounted for.
- High temperature and fO_2 allow stronger H₂O uptake into the garnet, while compositional effects are weak. Conversely, silica-undersaturation and high Al₂O₃ in clinopyroxene, typical for eclogites with strong plagioclase-rich cumulate protolith character (positive Eu anomalies, low ΣHREE abundances, low δ¹⁸O), facilitate H₂O uptake into clinopyroxene, whereas temperature- fO_2 effects are weak to absent.
- Clinopyroxene-garnet H₂O partition coefficients D in eclogite xenoliths range from 2.2 to 240, and in contrast to absolute H₂O abundances in garnet, show similar dependence on garnet Ca# and temperature as do incompatible trace elements and Fe³⁺/ΣFe. Correlations of $D(H_2O)$ with $D(TiO_2)$ imply that bulk eclogite H₂O abundance may be calculated from the distribution of these elements if the H₂O concentration in either clinopyroxene or garnet is known.
- H₂O contents in eclogite xenoliths in this study show no evidence for having been modified during entrainment in the host magma or by mantle metasomatism. They also differ from those reported for peridotite xenoliths from the same localities, suggesting that diffusive H₂O re-equilibration has not taken place. Primary H₂O may be retained because eclogite xenoliths are typically coarse-grained and entrained from presumably km-sized pods in the dominantly peridotitic cratonic lithosphere.
- Given their low estimated abundance in the cratonic mantle, calculated V_p (8.4–8.8 km/s) in Siberian eclogites are not high enough to explain the high velocities determined for this craton geophysically (up to 8.9 km/s), while calculated densities (3.53–3.71 g/cm³) may significantly contribute to the gravity signal. Electrical conductivities (10^{-4.7}–10^{-2.4} S/m) and, weakly, bulk H₂O abundances increase with depth and lie mostly between those of the relatively conductive Slave cratonic mantle and the more resistive Kaapvaal cratonic mantle. In the Siberian craton, where H₂O abundances in peridotite xenoliths also increase with depth, this may constitute a rheologically unfavorable combination for craton preservation.
- When combined with literature data, samples with plagioclase-rich, deep oceanic crustal protoliths have the highest bulk $c(H_2O)$. Given the increase in H₂O content with increasing Al₂O₃ in clinopyroxene, which requires the stabilization of the omphacite component during high-pressure metamorphism, this observation is ascribed to interaction of serpentinite-derived fluids, which are liberated at sufficiently great depths, with adjacent eclogitized gabbros. This deep crustal lithology has the greatest potential as a vector for deep H₂O recycling.
- The ancient bulk oceanic crust has an estimated $c(H_2O)$ of ~240 wt.ppm, which is similar to published estimates for modern subducted oceanic crust based on its electric resistivity, suggesting that the recycling efficiency of H₂O in subducting oceanic crust has not significantly changed since the Archean. This may place upper limits on convecting mantle T_p as one important variable dictating the dehydration of subducting slabs, and may have acted against the dehydration of the ancient mantle and against a gross imbalance between H₂O ingassing and outgassing through time.

Data Availability Statement

All data for this manuscript (H_2O concentrations and O isotope composition) are available at Aulbach et al. (2023).

Acknowledgments

Discussions with Nils Gies are much appreciated. Larry Heaman is thanked for provision of the Diavik xenoliths. We thank the editor, Whitney Behr, for seamless editorial handling, and two anonymous reviewers for their comments, which helped improve the clarity of the paper. This work was supported by the Deutsche Forschungsgemeinschaft (DFG, German Research Foundation)—Project number 432249855 (AU356/11) to SA, and by the state assignment Project IGM SB RAS (122041400241-5) to AK. Open Access funding enabled and organized by Projekt DEAL.

References

- Abers, G. A., & Hacker, B. R. (2016). A MATLAB toolbox and Excel workbook for calculating the densities, seismic wave speeds, and major element composition of minerals and rocks at pressure and temperature. *Geochemistry, Geophysics, Geosystems*, 17(2), 616–624. <https://doi.org/10.1002/2015gc006171>
- Agard, P., Yamato, P., Jolivet, L., & Burov, E. (2009). Exhumation of oceanic blueschists and eclogites in subduction zones: Timing and mechanisms. *Earth-Science Reviews*, 92(1), 53–79. <https://doi.org/10.1016/j.earscirev.2008.11.002>
- Agashev, A. M., Pokhilenko, L. N., Pokhilenko, N. P., & Shchukina, E. V. (2018). Geochemistry of eclogite xenoliths from the Udachnaya Kimberlite Pipe: Section of ancient oceanic crust sampled. *Lithos*, 314, 187–200. <https://doi.org/10.1016/j.lithos.2018.05.027>
- Agasheva, E. V., Kolesnichenko, M. V., Malygina, E. V., Agashev, A. M., & Zedgenizov, D. A. (2021). Origin of water in mantle eclogites from the V. Grib kimberlite pipe, NW Russia. *Lithosphere*, 2021(1), 7866657. <https://doi.org/10.2113/2021/7866657>
- Alt, J. C., Garrido, C. J., Shanks, W. C., Turchyn, A., Padrón-Navarta, J. A., López Sánchez-Vizcaíno, V., et al. (2012). Recycling of water, carbon, and sulfur during subduction of serpentinites: A stable isotope study of Cerro del Almiraz, Spain. *Earth and Planetary Science Letters*, 327–328, 50–60. <https://doi.org/10.1016/j.epsl.2012.01.029>
- Andrault, D., & Bolfan-Casanova, N. (2022). Mantle rain toward the Earth's surface: A model for the internal cycle of water. *Physics of the Earth and Planetary Interiors*, 322, 106815. <https://doi.org/10.1016/j.pepi.2021.106815>
- Antweiler, R. C. (2015). Evaluation of statistical treatments of left-censored environmental data using coincident uncensored data sets. II. Group comparisons. *Environmental Science & Technology*, 49(22), 13439–13446. <https://doi.org/10.1021/acs.est.5b02385>
- Arevalo, R., & McDonough, W. F. (2010). Chemical variations and regional diversity observed in MORB. *Chemical Geology*, 271(1–2), 70–85. <https://doi.org/10.1016/j.chemgeo.2009.12.013>
- Artemieva, I. M., Thybo, H., & Cherepanova, Y. (2019). Isopycnicity of cratonic mantle restricted to kimberlite provinces. *Earth and Planetary Science Letters*, 505, 13–19. <https://doi.org/10.1016/j.epsl.2018.09.034>
- Ashchepkov, I. V., Logvinova, A. M., Ntaflos, T., Vladykin, N. V., Kostrovitsky, S. I., Spetsius, Z., et al. (2017). Alakit and Daldyn kimberlite fields, Siberia, Russia: Two types of mantle sub-terraces beneath central Yakutia? *Geoscience Frontiers*, 8(4), 671–692. <https://doi.org/10.1016/j.gsf.2016.08.004>
- Aubaud, C., Hauri, E. H., & Hirschmann, M. M. (2004). Hydrogen partition coefficients between nominally anhydrous minerals and basaltic melts. *Geophysical Research Letters*, 31(20), L20611. <https://doi.org/10.1029/2004gl021341>
- Aubaud, C., Hirschmann, M. M., Withers, A. C., & Hervig, R. L. (2008). Hydrogen partitioning between melt, clinopyroxene, and garnet at 3 GPa in a hydrous MORB with 6 wt.% H_2O . *Contributions to Mineralogy and Petrology*, 156(5), 607–625. <https://doi.org/10.1007/s00410-008-0304-2>
- Aulbach, S. (2020). Temperature-dependent rutile solubility in garnet and clinopyroxene from mantle eclogite: Implications for continental crust formation and V-based oxybarometry. *Journal of Petrology*, 61(6), egaa065. <https://doi.org/10.1093/petrology/egaa065>
- Aulbach, S., & Arndt, N. T. (2019). Eclogites as palaeodynamic archives: Evidence for warm (not hot) and depleted (but heterogeneous) Archaean ambient mantle. *Earth and Planetary Science Letters*, 505, 162–172. <https://doi.org/10.1016/j.epsl.2018.10.025>
- Aulbach, S., Creaser, R. A., Pearson, N. J., Simonetti, S. S., Heaman, L. M., Griffin, W. L., & Stachel, T. (2009). Sulfide and whole rock Re-Os systematics of eclogite and pyroxenite xenoliths from the Slave craton, Canada. *Earth and Planetary Science Letters*, 283(1–4), 48–58. <https://doi.org/10.1016/j.epsl.2009.03.023>
- Aulbach, S., & Jacob, D. E. (2016). Major- and trace-elements in cratonic mantle eclogites and pyroxenites reveal heterogeneous sources and metamorphic processing of low-pressure protoliths. *Lithos*, 262, 586–605. <https://doi.org/10.1016/j.lithos.2016.07.026>
- Aulbach, S., Massuyeau, M., Garber, J. M., Gerdes, A., Heaman, L. M., & Viljoen, K. S. (2020). Ultramafic carbonated melt- and auto-metasomatism in mantle eclogites: Compositional effects and geophysical consequences. *Geochemistry, Geophysics, Geosystems*, 21(5), e2019GC008774. <https://doi.org/10.1029/2019gc008774>
- Aulbach, S., & Smart, K. A. (2023). Petrogenesis and geodynamic significance of xenolithic eclogites. *Annual Review of Earth and Planetary Sciences*, 51(1), 521–549. <https://doi.org/10.1146/annurev-earth-031621-112904>
- Aulbach, S., Stalder, R., & Stern, R. A. (2023). H_2O analyses of clinopyroxene and garnet (FTIR) and oxygen isotope analyses of garnet (SIMS) in eclogite xenoliths from Udachnaya (Siberian craton), version 1.0 [Dataset]. Interdisciplinary Earth Data Alliance (IEDA). <https://doi.org/10.26022/IEDA/113055>
- Aulbach, S., Woodland, A. B., Stagno, V., Korsakov, A. V., Mikhailenko, D., & Golovin, A. (2022). Fe^{3+} distribution and $Fe^{3+}/\Sigma Fe$ -oxygen fugacity variations in kimberlite-borne eclogite xenoliths, with comments on clinopyroxene-garnet oxy-thermobarometry. *Journal of Petrology*, 63(8), egac076. <https://doi.org/10.1093/petrology/egac076>
- Aulbach, S., Woodland, A. B., Stern, R. A., Vasilyev, P., Heaman, L. M., & Viljoen, K. S. (2019). Evidence for a dominantly reducing Archaean ambient mantle from two redox proxies, and low oxygen fugacity of deeply subducted oceanic crust. *Scientific Reports*, 9(1), 20190. <https://doi.org/10.1038/s41598-019-55743-1>
- Barnes, J. D., Selverstone, J., & Sharp, Z. D. (2006). Chlorine isotope chemistry of serpentinites from Elba, Italy, as an indicator of fluid source and subsequent tectonic history. *Geochemistry, Geophysics, Geosystems*, 7(8), Q08015. <https://doi.org/10.1029/2006gc001296>
- Bascou, J., Doucet, L. S., Saumet, S., Ionov, D. A., Ashchepkov, I. V., & Golovin, A. V. (2011). Seismic velocities, anisotropy and deformation in Siberian cratonic mantle: EBSD data on xenoliths from the Udachnaya kimberlite. *Earth and Planetary Science Letters*, 304(1–2), 71–84. <https://doi.org/10.1016/j.epsl.2011.01.016>
- Bell, D. R., Ihinger, P. D., & Rossman, G. R. (1995). Quantitative analysis of trace OH in garnet and pyroxenes. *American Mineralogist*, 80(5–6), 465–474. <https://doi.org/10.2138/am-1995-5-607>
- Bettac, S. P., Unsworth, M. J., Pearson, D. G., & Craven, J. (2023). New constraints on the structure and composition of the lithospheric mantle beneath the Slave craton, NW Canada from 3-D magnetotelluric data – Origin of the Central Slave Mantle Conductor and possible evidence for lithospheric scale fluid flow. *Tectonophysics*, 851, 229760. <https://doi.org/10.1016/j.tecto.2023.229760>
- Bleeker, W. (2002). Archaean tectonics: A review, with illustrations from the Slave craton. In C. M. R. Fowler, C. J. Ebinger, & C. J. Hawkesworth (Eds.), *The early Earth: Physical, chemical and biological development* (pp. 151–181). Geological Society, London, Special Publications.
- Cherepanova, Y., & Artemieva, I. M. (2015). Density heterogeneity of the cratonic lithosphere: A case study of the Siberian craton. *Gondwana Research*, 28(4), 1344–1360. <https://doi.org/10.1016/j.gr.2014.10.002>

- Coogan, L. A. (2014). 4.14 - The lower oceanic crust. In H. D. Holland & K. K. Turekian (Eds.), *Treatise on Geochemistry* (2nd ed., pp. 497–541). Elsevier.
- Creaser, R. A., Grütter, H., Carlson, J., & Crawford, B. (2004). Macrocrystal phlogopite Rb-Sr dates for the Ekati property kimberlites, Slave Province, Canada: evidence for multiple intrusive episodes in the Paleocene and Eocene. *Lithos*, *76*(1–4), 399–414. <https://doi.org/10.1016/j.lithos.2004.03.039>
- Dai, L., Hu, H., Li, H., Wu, L., Hui, K., Jiang, J., & Sun, W. (2016). Influence of temperature, pressure, and oxygen fugacity on the electrical conductivity of dry eclogite, and geophysical implications. *Geochemistry, Geophysics, Geosystems*, *17*(6), 2394–2407. <https://doi.org/10.1002/2016gc006282>
- Dai, L., & Karato, S. I. (2009). Electrical conductivity of orthopyroxene: Implications for the water content of the asthenosphere. *Proceedings of the Japan Academy Series B-Physical and Biological Sciences*, *85*(10), 466–475. <https://doi.org/10.2183/pjab.85.466>
- Davis, W. J., Jones, A. G., Bleeker, W., & Grutter, H. (2003). Lithosphere development in the Slave craton: A linked crustal and mantle perspective. *Lithos*, *71*(2–4), 575–589. [https://doi.org/10.1016/s0024-4937\(03\)00131-2](https://doi.org/10.1016/s0024-4937(03)00131-2)
- Demouchy, S. (2010). Diffusion of hydrogen in olivine grain boundaries and implications for the survival of water-rich zones in the Earth's mantle. *Earth and Planetary Science Letters*, *295*(1), 305–313. <https://doi.org/10.1016/j.epsl.2010.04.019>
- Demouchy, S., & Bolfan-Casanova, N. (2016). Distribution and transport of hydrogen in the lithospheric mantle: A review. *Lithos*, *240*, 402–425. <https://doi.org/10.1016/j.lithos.2015.11.012>
- Demouchy, S., Jacobsen, S. D., Gaillard, F., & Stern, C. R. (2006). Rapid magma ascent recorded by water diffusion profiles in mantle olivine. *Geology*, *34*(6), 429–432. <https://doi.org/10.1130/g22386.1>
- Denis, C. M. M., Alard, O., & Demouchy, S. (2015). Water content and hydrogen behaviour during metasomatism in the uppermost mantle beneath Ray Pic volcano (Massif Central, France). *Lithos*, *236–237*, 256–274. <https://doi.org/10.1016/j.lithos.2015.08.013>
- Dong, J., Fischer, R. A., Stixrude, L. P., & Lithgow-Bertelloni, C. R. (2021). Constraining the volume of Earth's early oceans with a temperature-dependent mantle water storage capacity model. *AGU Advances*, *2*(1), e2020AV000323. <https://doi.org/10.1029/2020av000323>
- Doucet, L. S., Ionov, D. A., & Golovin, A. V. (2013). The origin of coarse garnet peridotites in cratonic lithosphere: New data on xenoliths from the Udachnaya kimberlite, central Siberia. *Contributions to Mineralogy and Petrology*, *165*(6), 1225–1242. <https://doi.org/10.1007/s00410-013-0855-8>
- Doucet, L. S., Ionov, D. A., & Golovin, A. V. (2015). Paleoproterozoic formation age for the Siberian cratonic mantle: Hf and Nd isotope data on refractory peridotite xenoliths from the Udachnaya kimberlite. *Chemical Geology*, *391*, 42–55. <https://doi.org/10.1016/j.chemgeo.2014.10.018>
- Doucet, L. S., Peslier, A. H., Ionov, D. A., Brandon, A. D., Golovin, A. V., Goncharov, A. G., & Ashchepkov, I. V. (2014). High water contents in the Siberian cratonic mantle linked to metasomatism: An FTIR study of Udachnaya peridotite xenoliths. *Geochimica et Cosmochimica Acta*, *137*, 159–187. <https://doi.org/10.1016/j.gca.2014.04.011>
- Gale, A., Dalton, C. A., Langmuir, C. H., Su, Y., & Schilling, J.-G. (2013). The mean composition of ocean ridge basalts. *Geochemistry, Geophysics, Geosystems*, *14*(3), 489–518. <https://doi.org/10.1029/2012gc004334>
- Garber, J. M., Maurya, S., Hernandez, J., Duncan, M. S., Zeng, L., Zhang, H. L., et al. (2018). Multidisciplinary constraints on the abundance of diamond and eclogite in the cratonic lithosphere. *Geochemistry, Geophysics, Geosystems*, *19*(7), 2062–2086. <https://doi.org/10.1029/2018gc007534>
- Gose, J., & Schmädicke, E. (2018). Water incorporation in garnet: Coesite versus quartz eclogite from Erzgebirge and Fichtelgebirge. *Journal of Petrology*, *59*(2), 207–231. <https://doi.org/10.1093/petrology/egy022>
- Green, D. H., Hibberson, W. O., Kovacs, I., & Rosenthal, A. (2010). Water and its influence on the lithosphere-asthenosphere boundary. *Nature*, *467*(7314), 448–451. <https://doi.org/10.1038/nature09369>
- Gregory, R. T., & Taylor, H. P. (1981). An oxygen isotope profile in a section of cretaceous oceanic crust, Samail ophiolite, Oman – Evidence for ^{18}O buffering of the oceans by deep (>5 km) seawater-hydrothermal circulation at mid-ocean ridges. *Journal of Geophysical Research*, *86*(NB4), 2737–2755. <https://doi.org/10.1029/jb086ib04p02737>
- Griffin, W. L., Ryan, C. G., Kaminsky, F. V., O'Reilly, S. Y., Natapov, L. M., Win, T. T., et al. (1999). The Siberian lithosphere traverse: Mantle terranes and the assembly of the Siberian craton. *Tectonophysics*, *310*(1–4), 1–35. [https://doi.org/10.1016/s0040-1951\(99\)00156-0](https://doi.org/10.1016/s0040-1951(99)00156-0)
- Hammer, V. M. F., & Beran, A. (1991). Variations in the OH concentration of rutiles from different geological environments. *Mineralogy and Petrology*, *45*, 1–9. <https://doi.org/10.1007/bf01164498>
- Hardman, M. F., Stachel, T., Pearson, D. G., Cano, E. J., Stern, R. A., & Sharp, Z. D. (2021). Characterising the distinct crustal protoliths of Roberts Victor type I and II eclogites. *Journal of Petrology*, *62*(12), egab090. <https://doi.org/10.1093/petrology/egab090>
- Harte, B., & Kirkley, M. B. (1997). Partitioning of trace elements between clinopyroxene and garnet: Data from mantle eclogites. *Chemical Geology*, *136*(1–2), 1–24. [https://doi.org/10.1016/s0009-2541\(96\)00127-1](https://doi.org/10.1016/s0009-2541(96)00127-1)
- Hasterok, D., & Chapman, D. S. (2011). Heat production and geotherms for the continental lithosphere. *Earth and Planetary Science Letters*, *307*(1–2), 59–70. <https://doi.org/10.1016/j.epsl.2011.04.034>
- Heaman, L. M., Kjarsgaard, B. A., & Creaser, R. A. (2004). The temporal evolution of North American kimberlites. *Lithos*, *76*(1–4), 377–397. <https://doi.org/10.1016/j.lithos.2004.03.047>
- Heaman, L. M., & Pearson, D. G. (2010). Nature and evolution of the Slave Province subcontinental lithospheric mantle. *Canadian Journal of Earth Sciences*, *47*(4), 369–388. <https://doi.org/10.1139/e09-046>
- Helmstaedt, H. (2009). Crust-mantle coupling revisited: The Archean Slave craton, NWT, Canada. *Lithos*, *112*, 1055–1068. <https://doi.org/10.1016/j.lithos.2009.04.046>
- Herzberg, C., Condie, K., & Korenaga, J. (2010). Thermal history of the Earth and its petrological expression. *Earth and Planetary Science Letters*, *292*(1–2), 79–88. <https://doi.org/10.1016/j.epsl.2010.01.022>
- Holland, T. J. B. (1980). The reaction albite = jadeite + quartz determined experimentally in the range 600–1200°C. *American Mineralogist*, *65*(1–2), 129–134.
- Huang, J.-X., Li, P., Griffin, W. L., Xia, Q.-K., Gréau, Y., Pearson, N. J., & O'Reilly, S. Y. (2014). Water contents of Roberts Victor xenolithic eclogites: Primary and metasomatic controls. *Contributions to Mineralogy and Petrology*, *168*(6), 1092. <https://doi.org/10.1007/s00410-014-1092-5>
- Ickert, R. B., Stachel, T., Stern, R. A., & Harris, J. W. (2013). Diamond from recycled crustal carbon documented by coupled $\delta^{18}\text{O}$ - $\delta^{13}\text{C}$ measurements of diamonds and their inclusions. *Earth and Planetary Science Letters*, *364*, 85–97. <https://doi.org/10.1016/j.epsl.2013.01.008>
- Ickert, R. B., & Stern, R. A. (2013). Matrix corrections and error analysis in high-precision SIMS $^{18}\text{O}/^{16}\text{O}$ measurements of Ca-Mg-Fe garnet. *Geostandards and Geoanalytical Research*, *37*(4), 429–448. <https://doi.org/10.1111/j.1751-908x.2013.00222.x>
- Ingrin, J., & Skogby, H. (2000). Hydrogen in nominally anhydrous upper-mantle minerals: Concentration levels and implications. *European Journal of Mineralogy*, *12*(3), 543–570. <https://doi.org/10.1127/ejm/12/3/0543>

- Ionov, D. A., Carlson, R. W., Doucet, L. S., Golovin, A. V., & Oleinikov, O. B. (2015). The age and history of the lithospheric mantle of the Siberian craton: Re-Os and PGE study of peridotite xenoliths from the Obnazhennaya kimberlite. *Earth and Planetary Science Letters*, 428, 108–119. <https://doi.org/10.1016/j.epsl.2015.07.007>
- Ionov, D. A., Doucet, L. S., & Ashchepkov, I. V. (2010). Composition of the lithospheric mantle in the Siberian craton: New constraints from fresh peridotites in the Udachnaya-East kimberlite. *Journal of Petrology*, 51(11), 2177–2210. <https://doi.org/10.1093/ptrology/egq053>
- Ionov, D. A., Doucet, L. S., Carlson, R. W., Golovin, A. V., & Korsakov, A. V. (2015). Post-archean formation of the lithospheric mantle in the central Siberian craton: Re-Os and PGE study of peridotite xenoliths from the Udachnaya kimberlite. *Geochimica et Cosmochimica Acta*, 165, 466–483. <https://doi.org/10.1016/j.gca.2015.06.035>
- Ionov, D. A., Liu, Z., Li, J., Golovin, A. V., Korsakov, A. V., & Xu, Y. (2020). The age and origin of cratonic lithospheric mantle: Archean dunites vs. Paleoproterozoic harzburgites from the Udachnaya kimberlite, Siberian craton. *Geochimica et Cosmochimica Acta*, 281, 67–90. <https://doi.org/10.1016/j.gca.2020.05.009>
- Jacob, D. E. (2004). Nature and origin of eclogite xenoliths from kimberlites. *Lithos*, 77(1–4), 295–316. <https://doi.org/10.1016/j.lithos.2004.03.038>
- Jacob, D. E., Jagoutz, E., Lowry, D., Matthey, D., & Kudrjavitseva, G. (1994). Diamondiferous eclogites from Siberia - Remnants of Archean oceanic crust. *Geochimica et Cosmochimica Acta*, 58(23), 5191–5207. [https://doi.org/10.1016/0016-7037\(94\)90304-2](https://doi.org/10.1016/0016-7037(94)90304-2)
- Jacob, D. E., Viljoen, K. S., & Grassineau, N. V. (2009). Eclogite xenoliths from Kimberley, South Africa - A case study of mantle metasomatism in eclogites. *Lithos*, 112, 1002–1013. <https://doi.org/10.1016/j.lithos.2009.03.034>
- Jarrard, R. D. (2003). Subduction fluxes of water, carbon dioxide, chlorine, and potassium. *Geochemistry, Geophysics, Geosystems*, 4(5), 8905. <https://doi.org/10.1029/2002gc000392>
- Jerde, E. A., Taylor, L. A., Crozaz, G., & Sobolev, N. V. (1993). Exsolution of garnet within clinopyroxene of mantle eclogites - Major-element and trace-element chemistry. *Contributions to Mineralogy and Petrology*, 114(2), 148–159. <https://doi.org/10.1007/bf00307752>
- Jones, A. G., Evans, R. L., & Eaton, D. W. (2009). Velocity-conductivity relationships for mantle mineral assemblages in Archean cratonic lithosphere based on a review of laboratory data and Hashin-Shtrikman extremal bounds. *Lithos*, 109(1–2), 131–143. <https://doi.org/10.1016/j.lithos.2008.10.014>
- Jones, A. G., Ferguson, I. J., Chave, A. D., Evans, R. L., & McNeice, G. W. (2001). Electric lithosphere of the Slave craton. *Geology*, 29(5), 423–426. [https://doi.org/10.1130/0091-7613\(2001\)029<0423:elotsc>2.0.co;2](https://doi.org/10.1130/0091-7613(2001)029<0423:elotsc>2.0.co;2)
- Kamenetsky, V. S., Golovin, A. V., Maas, R., Giuliani, A., Kamenetsky, M. B., & Weiss, Y. (2014). Towards a new model for kimberlite petrogenesis: Evidence from unaltered kimberlites and mantle minerals. *Earth-Science Reviews*, 139, 145–167. <https://doi.org/10.1016/j.earscirev.2014.09.004>
- Kamenetsky, V. S., Kamenetsky, M. B., Golovin, A. V., Sharygin, V. V., & Maas, R. (2012). Ultrafresh salty kimberlite of the Udachnaya-East pipe (Yakutia, Russia): A petrological oddity or fortuitous discovery? *Lithos*, 152, 173–186. <https://doi.org/10.1016/j.lithos.2012.04.032>
- Katayama, I., Nakashima, S., & Yurimoto, H. (2006). Water content in natural eclogite and implication for water transport into the deep upper mantle. *Lithos*, 86(3), 245–259. <https://doi.org/10.1016/j.lithos.2005.06.006>
- Kessel, R., Schmidt, M. W., Ulmer, P., & Pettko, T. (2005). Trace element signature of subduction-zone fluids, melts and supercritical liquids at 120–180 km depth. *Nature*, 437(7059), 724–727. <https://doi.org/10.1038/nature03971>
- Kilgore, M. L., Peslier, A. H., Brandon, A. D., Schaffer, L. A., Morris, R. V., Graff, T. G., et al. (2020). Metasomatic control of hydrogen contents in the layered cratonic mantle lithosphere sampled by Lac de Gras xenoliths in the central Slave craton, Canada. *Geochimica et Cosmochimica Acta*, 286, 29–53. <https://doi.org/10.1016/j.gca.2020.07.013>
- Kitayama, Y., Thomassot, E., Galy, A., Golovin, A., Korsakov, A., d'Eyrames, E., et al. (2017). Co-Magmatic sulfides and sulfates in the Udachnaya-East pipe (Siberia): A record of the redox state and isotopic composition of sulfur in kimberlites and their mantle sources. *Chemical Geology*, 455, 315–330. <https://doi.org/10.1016/j.chemgeo.2016.10.037>
- Kobussen, A. F., Christensen, N. I., & Thybo, H. (2006). Constraints on seismic velocity anomalies beneath the Siberian craton from xenoliths and petrophysics. *Tectonophysics*, 425(1–4), 123–135. <https://doi.org/10.1016/j.tecto.2006.07.008>
- Koch-Müller, M., Matsyuk, S. S., & Wirth, R. (2004). Hydroxyl in omphacites and omphacitic clinopyroxenes of upper mantle to lower crustal origin beneath the Siberian platform. *American Mineralogist*, 89(7), 921–931. <https://doi.org/10.2138/am-2004-0701>
- Kohlstedt, D. L. (2006). The role of water in high-temperature rock deformation. *Reviews in Mineralogy and Geochemistry*, 62(1), 377–396. <https://doi.org/10.2138/rmg.2006.62.16>
- Kolesnichenko, M. V., Zedgenizov, D. A., Litasov, K. D., Safonova, I. Y., & Ragozin, A. L. (2017). Heterogeneous distribution of water in the mantle beneath the central Siberian craton: Implications from the Udachnaya kimberlite pipe. *Gondwana Research*, 47, 249–266. <https://doi.org/10.1016/j.gr.2016.09.011>
- Kolesnichenko, M. V., Zedgenizov, D. A., Ragozin, A. L., Litasov, K. D., & Shatsky, V. S. (2018). The role of eclogites in the redistribution of water in the subcontinental mantle of the Siberian craton: Results of determination of the water content in minerals from the Udachnaya pipe eclogites. *Russian Geology and Geophysics*, 59(7), 763–779. <https://doi.org/10.1016/j.rgg.2018.07.004>
- Korenaga, J. (2011). Thermal evolution with a hydrating mantle and the initiation of plate tectonics in the early Earth. *Journal of Geophysical Research*, 116(B12), B12403. <https://doi.org/10.1029/2011jb008410>
- Korenaga, J., Planavsky, N. J., & Evans, D. A. D. (2017). Global water cycle and the coevolution of the Earth's interior and surface environment. *Philosophical Transactions of the Royal Society A: Mathematical, Physical & Engineering Sciences*, 375(2094), 20150393. <https://doi.org/10.1098/rsta.2015.0393>
- Korolev, N. M., Melnik, A. E., Li, X. H., & Skublov, S. G. (2018). The oxygen isotope composition of mantle eclogites as a proxy of their origin and evolution: A review. *Earth-Science Reviews*, 185, 288–300. <https://doi.org/10.1016/j.earscirev.2018.06.007>
- Kovács, I., Hermann, J., O'Neill, H. S. C., Gerald, J. F., Sambridge, M., & Horváth, G. (2008). Quantitative absorbance spectroscopy with unpolarized light: Part II. Experimental evaluation and development of a protocol for quantitative analysis of mineral IR spectra. *American Mineralogist*, 93(5–6), 765–778. <https://doi.org/10.2138/am.2008.2656>
- Krogh, E. J. (1988). The garnet-clinopyroxene Fe-Mg geothermometer - A reinterpretation of existing experimental data. *Contributions to Mineralogy and Petrology*, 99(1), 44–48. <https://doi.org/10.1007/bf00399364>
- Kushiro, I. (1969). Clinopyroxene solid solutions formed by reactions between diopside and plagioclase at high pressures. *Min Soc Amer Spec Paper*, 2, 179–191.
- Kusky, T. M., Li, J. H., & Tucker, R. D. (2001). The Archean Dongwanzi ophiolite complex, North China craton: 2.505-billion-year-old oceanic crust and mantle. *Science*, 292(5519), 1142–1145. <https://doi.org/10.1126/science.1059426>
- Le Pape, F., Jones, A. G., Jessell, M. W., Hogg, C., Siebenaller, L., Perrouy, S., et al. (2021). The nature of the southern West African craton lithosphere inferred from its electrical resistivity. *Precambrian Research*, 358, 106190. <https://doi.org/10.1016/j.precamres.2021.106190>
- Libowitzky, E., & Beran, A. (2006). The structure of hydrous species in nominally anhydrous minerals: Information from polarized IR spectroscopy. *Reviews in Mineralogy and Geochemistry*, 62(1), 29–52. <https://doi.org/10.2138/rmg.2006.62.2>

- Libowitzky, E., & Rossman, G. R. (1996). Principles of quantitative absorbance measurements in anisotropic crystals. *Physics and Chemistry of Minerals*, 23(6), 319–327. <https://doi.org/10.1007/bf00199497>
- Libowitzky, E., & Rossman, G. R. (1997). An IR absorption calibration for water in minerals. *American Mineralogist*, 82(11–12), 1111–1115. <https://doi.org/10.2138/am-1997-11-1208>
- Liu, H., & Yang, X. (2020). Solubility of hydroxyl groups in pyroxenes: Effect of oxygen fugacity at 0.2–3 GPa and 800–1200°C. *Geochimica et Cosmochimica Acta*, 286, 355–379. <https://doi.org/10.1016/j.gca.2020.07.034>
- Liu, H., Zhang, K., Ingrin, J., & Yang, X. (2021). Electrical conductivity of omphacite and garnet indicates limited deep water recycling by crust subduction. *Earth and Planetary Science Letters*, 559, 116784. <https://doi.org/10.1016/j.epsl.2021.116784>
- Liu, H., Zhu, Q., & Yang, X. (2019). Electrical conductivity of OH-bearing omphacite and garnet in eclogite: The quantitative dependence on water content. *Contributions to Mineralogy and Petrology*, 174(7), 57. <https://doi.org/10.1007/s00410-019-1593-3>
- Liu, Z., Ionov, D. A., Nimis, P., Xu, Y., He, P., & Golovin, A. V. (2022). Thermal and compositional anomalies in a detailed xenolith-based lithospheric mantle profile of the Siberian craton and the origin of seismic midlithosphere discontinuities. *Geology*, 50(8), 891–896. <https://doi.org/10.1130/g49947.1>
- Lu, R., & Keppeler, H. (1997). Water solubility in pyrope to 100 kbar. *Contributions to Mineralogy and Petrology*, 129(1), 35–42. <https://doi.org/10.1007/s004100050321>
- Magni, V., Bouilhol, P., & van Hunen, J. (2014). Deep water recycling through time. *Geochemistry, Geophysics, Geosystems*, 15(11), 4203–4216. <https://doi.org/10.1002/2014gc005525>
- Marshall, E. W., Lassiter, J. C., & Barnes, J. D. (2018). On the (mis)behavior of water in the mantle: Controls on nominally anhydrous mineral water content in mantle peridotites. *Earth and Planetary Science Letters*, 499, 219–229. <https://doi.org/10.1016/j.epsl.2018.07.033>
- Martin, L. A. J., Rubatto, D., Crépeyron, C., Hermann, J., Putlitz, B., & Vitale-Brovarone, A. (2014). Garnet oxygen analysis by SHRIMP-SI: Matrix corrections and application to high-pressure metasomatic rocks from Alpine Corsica. *Chemical Geology*, 374–375, 25–36. <https://doi.org/10.1016/j.chemgeo.2014.02.010>
- Matsyuk, S. S., Langer, K., & Hösch, A. (1998). Hydroxyl defects in garnets from mantle xenoliths in kimberlites of the Siberian platform. *Contributions to Mineralogy and Petrology*, 132(2), 163–179. <https://doi.org/10.1007/s004100050414>
- McDonough, W. F., & Sun, S. S. (1995). The composition of the Earth. *Chemical Geology*, 120(3–4), 223–253. [https://doi.org/10.1016/0009-2541\(94\)00140-4](https://doi.org/10.1016/0009-2541(94)00140-4)
- McGunnigle, J. P., Cano, E. J., Sharp, Z. D., Muehlenbachs, K., Cole, D., Hardman, M. F., et al. (2022). Triple oxygen isotope evidence for a hot Archean ocean. *Geology*, 50(9), 991–995. <https://doi.org/10.1130/g50230.1>
- McLean, H., Banas, A., Creighton, S., Whiteford, S., Luth, R. W., & Stachel, T. (2007). Garnet xenocrysts from the Diavik mine, NWT, Canada: Composition, color, and paragenesis. *The Canadian Mineralogist*, 45(5), 1131–1145. <https://doi.org/10.2113/gscanmin.45.5.1131>
- Melnik, E. A., Suvorov, V. D., Pavlov, E. V., & Mishenkina, Z. R. (2015). Seismic and density heterogeneities of lithosphere beneath Siberia: Evidence from the Craton long-range seismic profile. *Polar Science*, 9(1), 119–129. <https://doi.org/10.1016/j.polar.2014.09.002>
- Mikhailenko, D. S., Aulbach, S., Korsakov, A. V., Golovin, A. V., Malygina, E. V., Gerdes, A., et al. (2021). Origin of graphite–diamond-bearing eclogites from Udachnaya kimberlite pipe. *Journal of Petrology*, 62(8), egab033. <https://doi.org/10.1093/ptrology/egab033>
- Mikhailenko, D. S., Golovin, A., Korsakov, A., Aulbach, S., Gerdes, A., & Ragozin, A. (2020). Metasomatic evolution of Coesite-bearing diamondiferous eclogite from the Udachnaya kimberlite. *Minerals*, 10(4), 383. <https://doi.org/10.3390/min10040383>
- Mikhailenko, D. S., Korsakov, A. V., Zelenovskiy, P. S., & Golovin, A. V. (2016). Graphite–diamond relations in mantle rocks: Evidence from an eclogitic xenolith from the Udachnaya kimberlite (Siberian Craton). *American Mineralogist*, 101(9–10), 2155–2167. <https://doi.org/10.2138/am-2016-5657>
- Mikhailenko, D. S., Stagno, V., Korsakov, A. V., Andreozzi, G. B., Marras, G., Cerantola, V., & Malygina, E. V. (2020). Redox state determination of eclogite xenoliths from Udachnaya kimberlite pipe (Siberian craton), with some implications for the graphite/diamond formation. *Contributions to Mineralogy and Petrology*, 175(11), 107. <https://doi.org/10.1007/s00410-020-01748-3>
- Moine, B. N., Bolfan-Casanova, N., Radu, I. B., Ionov, D. A., Costin, G., Korsakov, A. V., et al. (2020). Molecular hydrogen in minerals as a clue to interpret δD variations in the mantle. *Nature Communications*, 11(1), 3604. <https://doi.org/10.1038/s41467-020-17442-8>
- Mookherjee, M., & Karato, S.-I. (2010). Solubility of water in pyrope-rich garnet at high pressures and temperature. *Geophysical Research Letters*, 37(3), L03310. <https://doi.org/10.1029/2009gl01289>
- Moreira, H., Dhuime, B., Ionov, D., Buzenchi, A., & Gusev, N. (2023). Hafnium isotope systematics of zircon in high-grade metamorphic rocks of the Anabar shield, Siberia: Radiogenic Hf without mantle input? *Chemical Geology*, 636, 121644. <https://doi.org/10.1016/j.chemgeo.2023.121644>
- Moyen, J. F., Paquette, J. L., Ionov, D. A., Gannoun, A., Korsakov, A. V., Golovin, A. V., & Moine, B. N. (2017). Paleoproterozoic rejuvenation and replacement of Archean lithosphere: Evidence from zircon U–Pb dating and Hf isotopes in crustal xenoliths at Udachnaya, Siberian craton. *Earth and Planetary Science Letters*, 457, 149–159. <https://doi.org/10.1016/j.epsl.2016.09.046>
- Muehlenbachs, K., & Clayton, R. N. (1972a). Oxygen isotope geochemistry of submarine greenstones. *Canadian Journal of Earth Sciences*, 9(5), 471–478. <https://doi.org/10.1139/e72-038>
- Muehlenbachs, K., & Clayton, R. N. (1972b). Oxygen isotope studies of fresh and weathered submarine basalts. *Canadian Journal of Earth Sciences*, 9(2), 172–184. <https://doi.org/10.1139/e72-014>
- Nimis, P., & Grütter, H. (2010). Internally consistent geothermometers for garnet peridotites and pyroxenites. *Contributions to Mineralogy and Petrology*, 159(3), 411–427. <https://doi.org/10.1007/s00410-009-0455-9>
- Novella, D., Frost, D. J., Hauri, E. H., Bureau, H., Raepsaet, C., & Roberge, M. (2014). The distribution of H₂O between silicate melt and nominally anhydrous peridotite and the onset of hydrous melting in the deep upper mantle. *Earth and Planetary Science Letters*, 400, 1–13. <https://doi.org/10.1016/j.epsl.2014.05.006>
- O'Neill, H. S. C., Berry, A. J., & Mallmann, G. (2018). The oxidation state of iron in Mid-Ocean Ridge Basaltic (MORB) glasses: Implications for their petrogenesis and oxygen fugacities. *Earth and Planetary Science Letters*, 504, 152–162. <https://doi.org/10.1016/j.epsl.2018.10.002>
- O'Reilly, S. Y., & Griffin, W. L. (1995). Trace-element partitioning between garnet and clinopyroxene in mantle-derived pyroxenites and eclogites – P–T–X controls. *Chemical Geology*, 121(1–4), 105–130. [https://doi.org/10.1016/0009-2541\(94\)00147-z](https://doi.org/10.1016/0009-2541(94)00147-z)
- Paul, J., & Ghosh, A. (2020). Evolution of cratons through the ages: A time-dependent study. *Earth and Planetary Science Letters*, 531, 115962. <https://doi.org/10.1016/j.epsl.2019.115962>
- Paulatto, M., Laigle, M., Galve, A., Charvis, P., Sapin, M., Bayrakci, G., et al. (2017). Dehydration of subducting slow-spread oceanic lithosphere in the Lesser Antilles. *Nature Communications*, 8(1), 15980. <https://doi.org/10.1038/ncomms15980>
- Pearson, D. G., Shirey, S. B., Carlson, R. W., Boyd, F. R., Pokhilenko, N. P., & Shimizu, N. (1995). Re–Os, Sm–Nd, Rb–Sr isotope evidence for thick Archean lithospheric mantle beneath the Siberian craton modified by multistage metasomatism. *Geochimica et Cosmochimica Acta*, 59(5), 959–977. [https://doi.org/10.1016/00167-0379\(50\)00143-](https://doi.org/10.1016/00167-0379(50)00143-)

- Pearson, D. G., Snyder, G. A., Shirey, S. B., Taylor, L. A., Carlson, R. W., & Sobolev, N. V. (1995). Archean Re-Os age for Siberian eclogites and constraints on Archean tectonics. *Nature*, 374(6524), 711–713. <https://doi.org/10.1038/374711a0>
- Penniston-Dorland, S. C., Kohn, M. J., & Manning, C. E. (2015). The global range of subduction zone thermal structures from exhumed blueschists and eclogites: Rocks are hotter than models. *Earth and Planetary Science Letters*, 428, 243–254. <https://doi.org/10.1016/j.epsl.2015.07.031>
- Peslier, A. H. (2010). A review of water contents of nominally anhydrous natural minerals in the mantles of Earth, Mars and the Moon. *Journal of Volcanology and Geothermal Research*, 197(1–4), 239–258. <https://doi.org/10.1016/j.jvolgeores.2009.10.006>
- Peslier, A. H., & Luhr, J. F. (2006). Hydrogen loss from olivines in mantle xenoliths from Simcoe (USA) and Mexico: Mafic alkalic magma ascent rates and water budget of the sub-continental lithosphere. *Earth and Planetary Science Letters*, 242(3–4), 302–319. <https://doi.org/10.1016/j.epsl.2005.12.019>
- Peslier, A. H., Schönbächler, M., Busemann, H., & Karato, S. I. (2017). Water in the Earth's interior: Distribution and origin. *Space Science Reviews*, 212(1–2), 743–810. <https://doi.org/10.1007/s11214-017-0387-z>
- Peslier, A. H., Woodland, A. B., Bell, D. R., & Lazarov, M. (2010). Olivine water contents in the continental lithosphere and the longevity of cratons. *Nature*, 467(7311), 78–81. <https://doi.org/10.1038/nature09317>
- Peslier, A. H., Woodland, A. B., Bell, D. R., Lazarov, M., & Lapen, T. J. (2012). Metasomatic control of water contents in the Kaapvaal cratonic mantle. *Geochimica et Cosmochimica Acta*, 97, 213–246. <https://doi.org/10.1016/j.gca.2012.08.028>
- Peslier, A. H., Woodland, A. B., & Wolff, J. A. (2008). Fast kimberlite ascent rates estimated from hydrogen diffusion profiles in xenolithic mantle olivines from southern Africa. *Geochimica et Cosmochimica Acta*, 72(11), 2711–2722. <https://doi.org/10.1016/j.gca.2008.03.019>
- Ponomarenko, A. I., Spetsius, Z. V., & Sobolev, N. V. (1980). New type of diamond-bearing rock — Garnet pyroxenite. *Doklady Akademii Nauk SSSR*, 251, 438–444.
- Radu, I. B., Moine, B., Ionov, D., Korsakov, A., Golovin, A., Mikhailenko, D., & Cottin, J. Y. (2017). Kyanite-bearing eclogite xenoliths from the Udachnaya kimberlite, Siberian craton, Russia. *Bulletin de la Societe Geologique de France*, 188(1–2), 7. <https://doi.org/10.1051/bsgf/2017008>
- Radu, I. B., Moine, B. N., Bolfan-Casanova, N., Ionov, D. A., Devidal, J. L., Delouie, E., et al. (2022). Zoisite in cratonic eclogite xenoliths - Implications for water in the upper mantle. *Lithos*, 418–419, 106681. <https://doi.org/10.1016/j.lithos.2022.106681>
- Ragozin, A. L., Karimova, A. A., Litasov, K. D., Zedgenizov, D. A., & Shatsky, V. S. (2014). Water content in minerals of mantle xenoliths from the Udachnaya pipe kimberlites (Yakutia). *Russian Geology and Geophysics*, 55(4), 428–442. <https://doi.org/10.1016/j.rgg.2014.03.002>
- Reynes, J., Lanari, P., & Hermann, J. (2020). A mapping approach for the investigation of Ti–OH relationships in metamorphic garnet. *Contributions to Mineralogy and Petrology*, 175(5), 46. <https://doi.org/10.1007/s00410-020-01681-5>
- Rudnick, R. L., & Fountain, D. M. (1995). Nature and composition of the continental crust - A lower crustal perspective. *Reviews of Geophysics*, 33(3), 267–309. <https://doi.org/10.1029/95rg01302>
- Rüpk, L. H., Morgan, J. P., Hort, M., & Connolly, J. A. D. (2004). Serpentine and the subduction zone water cycle. *Earth and Planetary Science Letters*, 223(1–2), 17–34. <https://doi.org/10.1016/j.epsl.2004.04.018>
- Russell, J. K., Dipple, G. M., & Kopylova, M. G. (2001). Heat production and heat flow in the mantle lithosphere, Slave craton, Canada. *Physics of the Earth and Planetary Interiors*, 123(1), 27–44. [https://doi.org/10.1016/s0031-9201\(00\)00201-6](https://doi.org/10.1016/s0031-9201(00)00201-6)
- Safronov, A. F., Nikishov, K. N., Botkunov, A. I., Gotovtsev, V. V., & Mahotko, V. F. (1980). Composition of garnets and pyroxenes from diamond-bearing eclogites from pipes Mir and Udachnaya. *Soviet Geology and Geophysics*, 21, 76–82.
- Schlechter, E., Stalder, R., & Behrens, H. (2012). Electrical conductivity of H-bearing orthopyroxene single crystals measured with impedance spectroscopy. *Physics and Chemistry of Minerals*, 39(7), 531–541. <https://doi.org/10.1007/s00269-012-0509-9>
- Schmidberger, S. S., Simonetti, A., Heaman, L. M., Creaser, R. A., & Whiteford, S. (2007). Lu-Hf, in-situ Sr and Pb isotope and trace element systematics for mantle eclogites from the Diavik diamond mine: Evidence for Paleoproterozoic subduction beneath the Slave craton, Canada. *Earth and Planetary Science Letters*, 254(1–2), 55–68. <https://doi.org/10.1016/j.epsl.2006.11.020>
- Schmidt, M. W., & Poli, S. (2014). Devolatilization during subduction. In H. D. Holland, K. K. Turekian, & R. L. Rudnick (Eds.), *Treatise on geochemistry 2nd edition - The crust* (pp. 669–701). Elsevier/Pergamon.
- Schulze, D. J. (1989). Constraints on the abundance of eclogite in the upper mantle. *Journal of Geophysical Research*, 94(B4), 4205–4212. <https://doi.org/10.1029/jb094ib04p04205>
- Selway, K. (2014). On the causes of electrical conductivity anomalies in tectonically stable lithosphere. *Surveys in Geophysics*, 35(1), 219–257. <https://doi.org/10.1007/s10712-013-9235-1>
- Shatsky, V. S., Zedgenizov, D. A., & Ragozin, A. L. (2016). Evidence for a subduction component in the diamond-bearing mantle of the Siberian craton. *Russian Geology and Geophysics*, 57(1), 111–126. <https://doi.org/10.1016/j.rgg.2016.01.008>
- Skogby, H., Bell, D. R., & Rossman, G. R. (1990). Hydroxide in pyroxene; variations in the natural environment. *American Mineralogist*, 75(7–8), 764–774.
- Smart, K. A., Heaman, L. M., Chacko, T., Simonetti, A., Kopylova, M., Mah, D., & Daniels, D. (2009). The origin of high-MgO diamond eclogites from the Jericho Kimberlite, Canada. *Earth and Planetary Science Letters*, 284(3–4), 527–537. <https://doi.org/10.1016/j.epsl.2009.05.020>
- Smart, K. A., Tappe, S., Woodland, A. B., Harris, C., Corcoran, L., & Simonetti, A. (2021). Metasomatized eclogite xenoliths from the central Kaapvaal craton as probes of a seismic mid-lithospheric discontinuity. *Chemical Geology*, 578, 120286. <https://doi.org/10.1016/j.chemgeo.2021.120286>
- Smyth, J. R., Bell, D. R., & Rossman, G. R. (1991). Incorporation of hydroxyl in upper-mantle clinopyroxenes. *Nature*, 351(6329), 732–735. <https://doi.org/10.1038/351732a0>
- Snyder, G. A., Taylor, L. A., Crozaz, G., Halliday, A. N., Beard, B. L., Sobolev, V. N., & Sobolev, N. V. (1997). The origins of Yakutian eclogite xenoliths. *Journal of Petrology*, 38(1), 85–113. <https://doi.org/10.1093/ptro/38.1.85>
- Snyder, G. A., Taylor, L. A., Jerde, E. A., Clayton, R. N., Mayeda, T. K., Deines, P., et al. (1995). Archean mantle heterogeneity and the origin of diamondiferous eclogites, Siberia - Evidence from stable isotopes and hydroxyl in garnet. *American Mineralogist*, 80(7–8), 799–809. <https://doi.org/10.2138/am-1995-7-816>
- Sobolev, N. V. (1977). Deep-seated inclusions in kimberlites and the problem of the composition of the upper mantle.
- Sobolev, N. V. (1990). Deep seated magmatism and evolution of lithosphere of the Siberian platform. In *International field seminar*. Institute of Geology and Geophysics, Siberian Branch of the Russian Academy of Sciences.
- Spetsius, Z. V. (1995). Occurrence of diamond in the mantle: A case study from the Siberian platform. *Journal of Geochemical Exploration*, 53(1), 25–39. [https://doi.org/10.1016/0375-6742\(94\)00022-4](https://doi.org/10.1016/0375-6742(94)00022-4)
- Spetsius, Z. V. (2004). Petrology of highly aluminous xenoliths from kimberlites of Yakutia. *Lithos*, 77(1–4), 525–538. <https://doi.org/10.1016/j.lithos.2004.04.021>
- Stachel, T., Aulbach, S., & Harris, J. W. (2022). *Mineral inclusions in lithospheric diamonds*. The Mineralogical Society of America.
- Stagno, V., Frost, D. J., McCammon, C. A., Mohseni, H., & Fei, Y. (2015). The oxygen fugacity at which graphite or diamond forms from carbonate-bearing melts in eclogitic rocks. *Contributions to Mineralogy and Petrology*, 169(2), 16. <https://doi.org/10.1007/s00410-015-1111-1>

- Stalder, R. (2004). Influence of Fe, Cr and Al on hydrogen incorporation in orthopyroxene. *European Journal of Mineralogy*, *16*(5), 703–711. <https://doi.org/10.1127/0935-1221/2004/0016-0703>
- Stalder, R., & Ludwig, T. (2007). OH incorporation in synthetic diopside. *European Journal of Mineralogy*, *19*(3), 373–380. <https://doi.org/10.1127/0935-1221/2007/0019-1721>
- Staudigel, H. (2005). Hydrothermal alteration processes in the oceanic crust. In H. D. Holland & K. K. Turekian (Eds.), *Treatise on Geochemistry. The crust* (pp. 511–535). Elsevier/Pergamon.
- Sun, J., Rudnick, R. L., Kostrovitsky, S., Kalashnikova, T., Kitajima, K., Li, R. P., & Shu, Q. (2020). The origin of low-MgO eclogite xenoliths from Obnazhennaya kimberlite, Siberian craton. *Contributions to Mineralogy and Petrology*, *175*(3), 25. <https://doi.org/10.1007/s00410-020-1655-6>
- Sun, S.-S., & McDonough, W. F. (1989). Chemical and isotopic systematics of oceanic basalts: Implications for mantle composition and processes. In A. D. Saunders & M. J. Norry (Eds.), *Magmatism in the ocean basins* (pp. 313–345). Geological Society.
- Sundvall, R., & Stalder, R. (2011). Water in upper mantle pyroxene megacrysts and xenocrysts: A survey study. *American Mineralogist*, *96*(8–9), 1215–1227. <https://doi.org/10.2138/am.2011.3641>
- Taylor, L. A., Logvinoya, A. M., Howarth, G. H., Liu, Y., Peslier, A. H., Rossman, G. R., et al. (2016). Low water contents in diamond mineral inclusions: Proto-genetic origin in a dry cratonic lithosphere. *Earth and Planetary Science Letters*, *433*, 125–132. <https://doi.org/10.1016/j.epsl.2015.10.042>
- van Hunen, J., & van den Berg, A. P. (2008). Plate tectonics on the early Earth: Limitations imposed by strength and buoyancy of subducted lithosphere. *Lithos*, *103*(1–2), 217–235. <https://doi.org/10.1016/j.lithos.2007.09.016>
- van Keken, P. E., Hacker, B. R., Syracuse, E. M., & Abers, G. A. (2011). Subduction factory: 4. Depth-dependent flux of H₂O from subducting slabs worldwide. *Journal of Geophysical Research*, *116*(B1), B01401. <https://doi.org/10.1029/2010jb007922>
- Wang, H. L., van Hunen, J., Pearson, D. G., & Allen, M. B. (2014). Craton stability and longevity: The roles of composition-dependent rheology and buoyancy. *Earth and Planetary Science Letters*, *391*, 224–233. <https://doi.org/10.1016/j.epsl.2014.01.038>
- Wang, Y., Wang, K., He, J., & Zhang, L. (2023). On unusual conditions for the exhumation of subducted oceanic crustal rocks: How to make rocks hotter than models. *Earth and Planetary Science Letters*, *615*, 118213. <https://doi.org/10.1016/j.epsl.2023.118213>
- Wenner, D. B., & Taylor, H. P. (1973). Oxygen and hydrogen isotope studies of the serpentinization of ultramafic rocks in oceanic environments and continental ophiolite complexes. *American Journal of Science*, *273*(3), 207–239. <https://doi.org/10.2475/ajs.273.3.207>
- White, W. M., & Klein, E. M. (2014). Composition of the oceanic crust. In H. D. Holland, K. K. Turekian, & R. W. Carlson (Eds.), *Treatise on Geochemistry* (2nd ed., pp. 457–496). Elsevier Pergamon.
- Xia, Q.-K., Liu, J., Kovács, I., Hao, Y.-T., Li, P., Yang, X.-Z., et al. (2019). Water in the upper mantle and deep crust of eastern China: Concentration, distribution and implications. *National Science Review*, *6*(1), 125–144. <https://doi.org/10.1093/nsr/nwx016>
- Yang, X. Z., & McCammon, C. (2012). Fe³⁺-rich augite and high electrical conductivity in the deep lithosphere. *Geology*, *40*(2), 131–134. <https://doi.org/10.1130/g32725.1>
- Zhang, K., Liu, H., Ionov, D. A., & Yang, X. (2022). Effects of oxygen fugacity on hydroxyl incorporation in garnet at 1–3 GPa and 800–1000°C and implications for water storage in the mantle. *Journal of Geophysical Research: Solid Earth*, *127*(4), e2022JB023948. <https://doi.org/10.1029/2022jb023948>
- Zhao, C. C., & Yoshino, T. (2016). Electrical conductivity of mantle clinopyroxene as a function of water content and its implication on electrical structure of uppermost mantle. *Earth and Planetary Science Letters*, *447*, 1–9. <https://doi.org/10.1016/j.epsl.2016.04.028>

References From the Supporting Information

- Alifirova, T. A., Pokhilenko, L. N., & Korsakov, A. V. (2015). Apatite, SiO₂, rutile and orthopyroxene precipitates in minerals of eclogite xenoliths from Yakutian kimberlites, Russia. *Lithos*, *226*, 31–49. <https://doi.org/10.1016/j.lithos.2015.01.020>
- Beyer, C., Frost, D. J., & Miyajima, N. (2015). Experimental calibration of a garnet-clinopyroxene geobarometer for mantle eclogites. *Contributions to Mineralogy and Petrology*, *169*(2), 18. <https://doi.org/10.1007/s00410-015-1113-z>
- Gardés, E., Gaillard, F., & Tarits, P. (2014). Toward a unified hydrous olivine electrical conductivity law. *Geochemistry, Geophysics, Geosystems*, *15*(12), 4984–5000. <https://doi.org/10.1002/2014gc005496>
- Grütter, H. S. (2009). Pyroxene xenocryst geotherms: Techniques and application. *Lithos*, *112*, 1167–1178. <https://doi.org/10.1016/j.lithos.2009.03.023>
- Konzett, J., Libowitzky, E., Hejny, C., Miller, C., & Zanetti, A. (2008). Oriented quartz+calcic amphibole inclusions in omphacite from the Saualpe and Pohorje mountain eclogites, eastern Alps—An assessment of possible formation mechanisms based on IR- and mineral chemical data and water storage in eastern Alpine eclogites. *Lithos*, *106*(3), 336–350. <https://doi.org/10.1016/j.lithos.2008.09.002>
- Laurie, A., Stevens, G., & van Hunen, J. (2013). The end of continental growth by TTG magmatism. *Terra Nova*, *25*(2), 130–136. <https://doi.org/10.1111/ter.12015>
- Nimis, P. (2022). Pressure and temperature data for diamonds. *Reviews in Mineralogy and Geochemistry*, *88*(1), 533–565. <https://doi.org/10.2138/rmg.2022.88.10>
- Pearson, N. J., Griffin, W. L., Doyle, B. J., O'Reilly, S. Y., van Acherbergh, E., & Kivi, K. (1999). Xenoliths from kimberlite pipes of the Lac de gas area, Slave craton, Canada. In *Paper presented at 7th Int Kimb Conf.*
- Schmädicke, E., & Gose, J. (2017). Water transport by subduction: Clues from garnet of Erzgebirge UHP eclogite. *American Mineralogist*, *102*(5), 975–986. <https://doi.org/10.2138/am-2017-5920>
- Spandler, C., & Pirard, C. (2013). Element recycling from subducting slabs to arc crust: A review. *Lithos*, *170*, 208–223. <https://doi.org/10.1016/j.lithos.2013.02.016>
- Stalder, R. (2021). OH point defects in quartz – A review. *European Journal of Mineralogy*, *33*(2), 145–163. <https://doi.org/10.5194/ejm-33-145-2021>
- Ziaja, K., Foley, S. F., White, R. W., & Buhre, S. (2014). Metamorphism and melting of picritic crust in the early Earth. *Lithos*, *189*, 173–184. <https://doi.org/10.1016/j.lithos.2013.07.001>